Politecnico di Torino

Fabrication of copper-based electrodes for the electrosynthesis of valuable products from carbon dioxide

Master of Science course in Nanotechnologies for ICTs

Author: Fausto Nevola

Supervisor: Fabrizio Pirri

Co-supervisor: Juqin Zeng

Co-supervisor: Felicia Di Costola

A.Y. 2024-2025

Contents

CHAPTER 1

Introduction

1.1 The problem of CO_2 emissions

Climate change represents one of the most pressing global challenges of the 21st century, largely driven by the continuous increase in atmospheric carbon dioxide (CO_2) levels due to human activities, as shown in Fig.1.1. This greenhouse gas is released mainly through fossil fuel combustion and industrial processes, such as the production of cement and steel [1], and its accumulation in the atmosphere has triggered serious environmental consequences and presents an urgent and potentially irreversible threat to human society, including global warming and extreme weather events [2]. Addressing this issue by achieving net zero CO_2 emissions before the middle of the century is essential to mitigate the most severe impacts of climate change; however, it requires not only massive implementation of renewable energy sources, but also developing strategies to capture and reuse CO_2 in a sustainable way [3].

1.2 CO_2 conversion as a sustainable approach

Among the different solutions under investigation for CO_2 conversion (see Fig.1.2), electrochemical reduction of carbon dioxide (CO_2RR) is one of the most promising approaches to recycle this greenhouse gas into chemical fuels and feedstocks [4],[5]. The electricity required for this process can be derived from renewable sources, so that the CO_2RR enables the storage of intermittent renewable energy in chemical form [6]. Since for many energy services in industrial value chains it is hard to use electricity directly, energy carriers will be needed. The higher the energy density value, the more useful a carrier becomes as an energy service supplier: they become easier to store and transport [7].

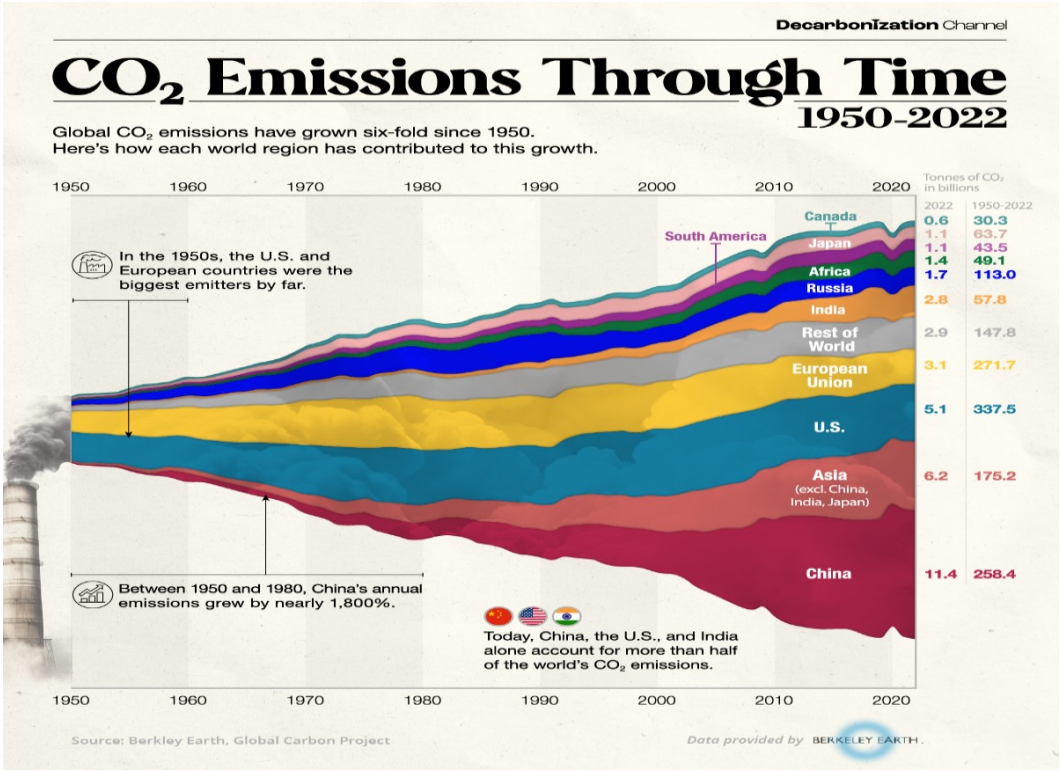

Figure 1.1: Global CO_2 emissions over the decades. [1]

For these reasons, CO_2 conversion using renewable energy sources represents an elegant long-term solution to climate change, in which value-added products such as hydrocarbons and oxygenates could be selectively produced [8],[9], as show in Fig.1.3. Compared with other approaches, namely thermochemical or photochemical conversion methods, electrochemical reduction (ECR) is one of the most promising strategies because of the mild operating conditions, high reaction efficiency, and modular reactor designs [10], which allows easy scalability to industrial applications while maintaining flexibility in reaction conditions and system design.

1.3 The challenge of CO_2 stability

Despite these promising features, several challenges still limit the practical application of CO_2RR. The first one, to obtain a cost-effective process, is the high energy requirement to break the double bonds (C=O) in the CO_2 molecules [13]. Since those molecules are thermodynamically stable and kinetically inert, a significant energy input is necessary as well as the presence of efficient catalysts to lower the activation barrier [14].

[1] https://decarbonization.visualcapitalist.com/global-co2-emissions-through-time-1950-2022/

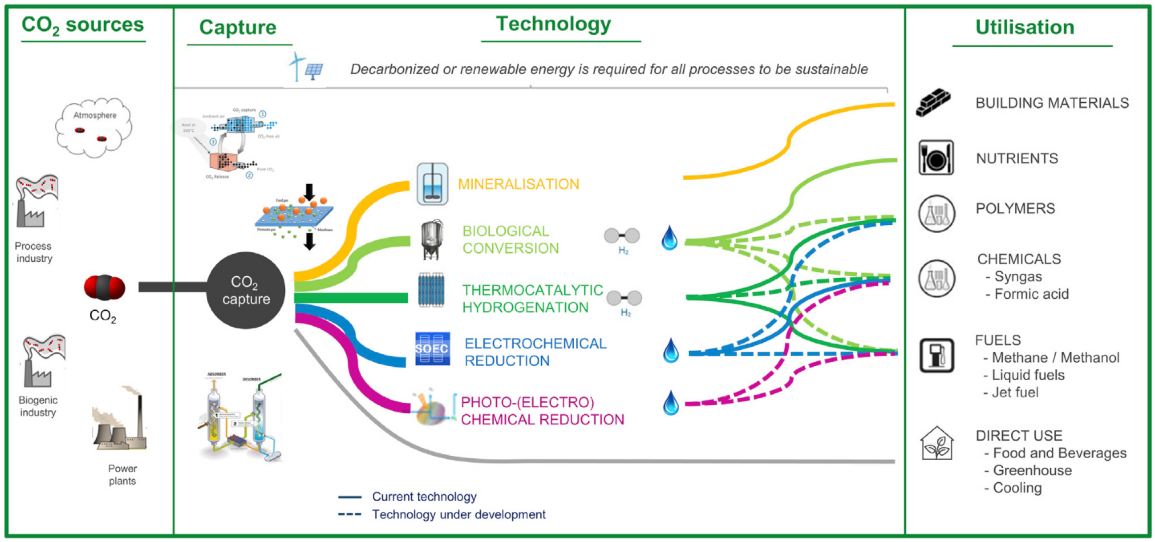

Figure 1.2: Different mechanisms for the CO_2 conversion [11].

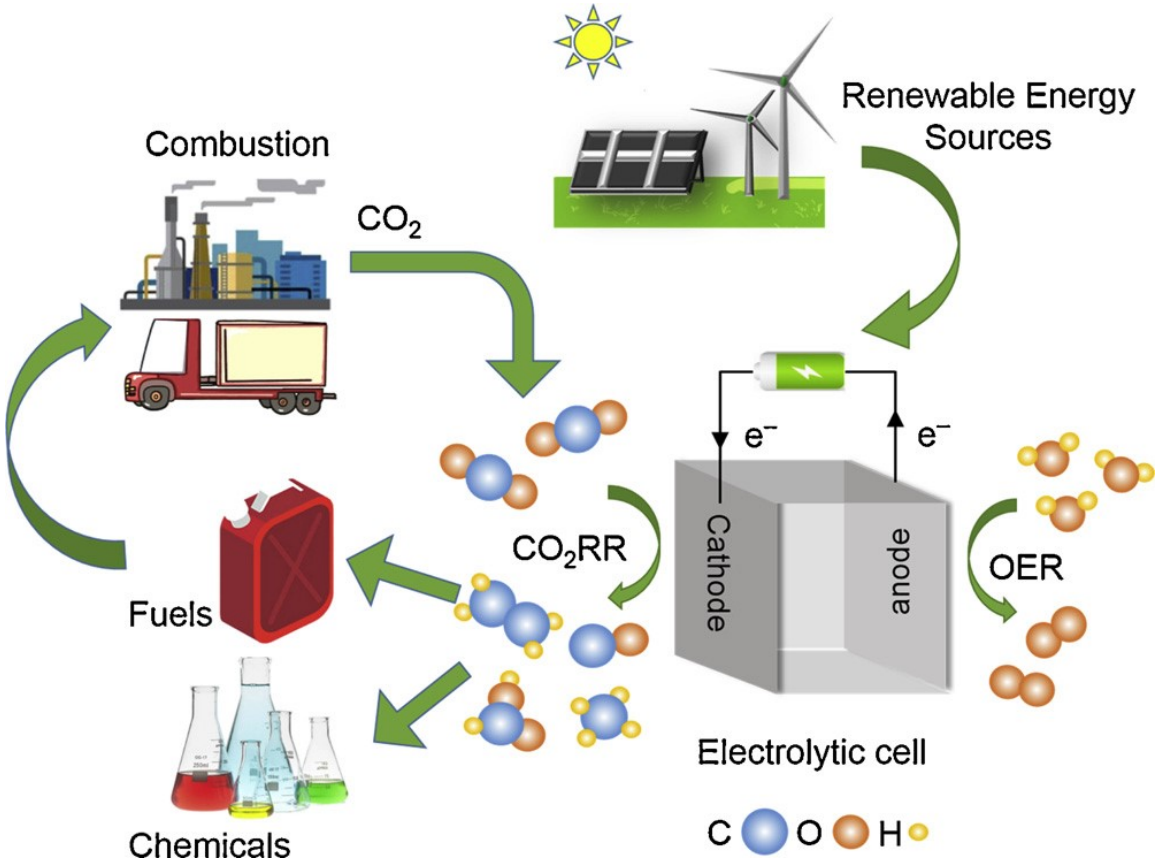

Figure 1.3: A schematic diagram of electrochemical CO_2 reduction to chemical fuels from clean energy sources [12].

In addition, the hydrogen evolution reaction (HER) competes with the CO_2RR under similar electrochemical conditions, thus further hindering its development toward industrial applications. This technology requires a careful selection of materials, as many catalysts exhibit low conversion selectivity and tend to suffer from performance degradation over time. Usually, the performance of electrocatalysis can be quantitatively measured for several fundamental parameters, such as the onset potential, the faradaic efficiency (FE), the energy efficiency and the current density [15]. The analysis of the latter gives feedback on the potential application of specific material for the CO2RR. For example, from these parameters, product selectivity can be evaluated by measuring the FEs and current densities [16]. Therefore, developing efficient, selective and stable catalysts is a key research priority for the CO_2 conversion.

1.4 Objective of the thesis

In this thesis work, copper (Cu)-based catalysts supported on commercial gas diffusion layer (GDL) carbon paper were fabricated by electrodeposition method, which is a simple, cost-effective and scalable technique for synthesizing catalytic films with controlled morphology and thickness. This process enabled the fabrication of free-standing gas diffusion electrodes (GDEs) by directly depositing the Cu catalyst onto the substrate. Furthermore, to explore the potential benefits of bimetallic systems, a part of the electrodes was subsequently modified with a displacement reaction in silver sulfate (Ag_2SO_4) aqueous solution. The prepared GDEs were then characterized with field-emission scanning electron microscopy (FESEM) and energy-dispersive spectroscopy (EDS), to study their surface morphology and elemental composition. Furthermore, they were tested in a membrane electrode assembly (MEA) cell configuration to evaluate their activity, selectivity and stability toward the CO_2RR. The amount of liquid and gaseous products were estimated with a high-performance liquid chromatograph (HPLC) and a micro-gas chromatograph (µGC) respectively. The resulting values were subsequently used to estimate the FEs of the reaction products and to assess the overall performance of the fabricated samples. The main objectives of this work can be summarized as follows:

1. To synthesize and characterize Cu electrodes fabricated with electrodeposition method on GDL carbon paper, giving particular consideration to the deposition reaction parameters.

2. To prepare Cu-Ag bimetallic electrodes via silver displacement and compare their physical and electrochemical properties with the monometallic ones.

3. To investigate the electrochemical performance of the fabricated electrodes in MEA systems, with emphasis on the relation between the deposition parameters and the obtained product selectivity.

1.5 Structure of the thesis

This thesis is organized into four chapters:

1. State of the art of current CO_2RR.
2. Materials and methods.
3. Results and discussion.
4. Conclusion and future perspectives.

CHAPTER 2

State of the art

This chapter presents an overview of the current state of the art in the CO_2RR, with a focus on the key scientific concepts and technological approaches that support the ongoing developments. A detailed analysis of the electrocatalytic process, along with the current employed catalyst materials, electrode design, and cell architecture, is provided.

2.1 Fundamentals of electrochemical CO_2 reduction

The CO_2RR has emerged as a promising strategy to mitigate greenhouse gas emission while producing renewable fuels and chemicals [17]. During this process, CO_2 molecules dissolved in an electrolyte are reduced under the influence of an applied potential and converted into value-added products [18]. While this mechanism occurs at the cathode, water oxidizes at the anode to supply the protons and electrons necessary for the reaction. However, CO_2 molecules have linear structures and strong C=O bonds (750 kJ/mol), which make them quite stable and kinetically inert, thus posing a significant challenge for their activation and subsequent reduction [19]. They possess a high activation barrier, which in turn leads to significant overpotentials [20], making the process energy-intensive and economically unfavorable. In addition, the CO_2RR proceeds through multiple reaction steps involving different numbers of protons and electrons, where various intermediates can evolve into different products [21], such as CO, methane (CH_4), formic acid (HCOOH) and alcohols. For these reasons, the use of reaction catalyst materials, capable of reducing the activation barrier and steering the products selectivity, is necessary. As many as 16 reaction products, ranging from hydrocarbons to oxygenates, have been identified for the CO_2RR in an aqueous electrolyte on Cu catalysts [22] (see Table2.1), leading to a wide variety but, nevertheless, low product selectivity. Unfortunately, the competing HER at cathode requires a lower overpotential than the CO_2 activation and tends to dominate, thus consuming the electrons and protons that would otherwise contribute to CO_2 conversion.

Finally, the generated oxygenates are usually mixed with solutes in the electrolyte, which then require extra separation and concentration processes to recover pure liquid fuel solutions in practical applications. At the same time, the evolved hydrocarbons are also mixed with H_2 and residual CO_2, making a costly separation process indispensable [23]. For these reasons, steering selectivity toward fewer desired products is one of the keys to industrial applications of the CO_2 conversion.

Table 2.1: Half electrochemical thermodynamic reactions of the main CO_2RR products, together with the corresponding standard redox potentials [23].

Products	Acid pH = 0		Base pH = 14	
	Equation	*E* (V vs. SHE)	Equation	*E* (V vs. SHE)
Hydrogen	$2H^+ + 2e^- \rightarrow H_2$	0.000	$2H_2O + 2e^- \rightarrow H_2 + 2OH^-$	−0.828
Carbon monoxide	$CO_2 + 2H^+ + 2e^- \rightarrow CO + H_2O$	−0.104	$CO_2 + H_2O + 2e^- \rightarrow CO + 2OH^-$	−0.932
Methane	$CO_2 + 8H^+ + 8e^- \rightarrow CH_4 + 2H_2O$	0.169	$CO_2 + 6H_2O + 8e^- \rightarrow CH_4 + 8OH^-$	−0.659
Methanol	$CO_2 + 6H^+ + 6e^- \rightarrow CH_3OH + H_2O$	0.016	$CO_2 + 5H_2O + 6e^- \rightarrow CH_3OH + 6OH^-$	−0.812
Formic acid/formate	$CO_2 + 2H^+ + 2e^- \rightarrow HCOOH$	−0.171	$CO_2 + H_2O + 2e^- \rightarrow HCOO^- + OH^-$	−0.639
Ethylene	$2CO_2 + 12H^+ + 12e^- \rightarrow C_2H_4 + 4H_2O$	0.085	$2CO_2 + 8H_2O + 12e^- \rightarrow C_2H_4 + 12OH^-$	−0.743
Ethane	$2CO_2 + 14H^+ + 14e^- \rightarrow C_2H_6 + 4H_2O$	0.144	$2CO_2 + 10H_2O + 14e^- \rightarrow C_2H_6 + 14OH^-$	−0.685
Ethanol	$2CO_2 + 12H^+ + 12e^- \rightarrow CH_3CH_2OH + 3H_2O$	0.084	$2CO_2 + 9H_2O + 12e^- \rightarrow CH_3CH_2OH + 12OH^-$	−0.744
Acetic acid/acetate	$2CO_2 + 8H^+ + 8e^- \rightarrow CH_3COOH + 2H_2O$	0.098	$2CO_2 + 5H_2O + 8e^- \rightarrow CH_3COO^- + 7OH^-$	−0.653
n-Propanol	$3CO_2 + 18H^+ + 18e^- \rightarrow CH_3CH_2CH_2OH + 5H_2O$	0.095	$3CO_2 + 13H_2O + 18e^- \rightarrow CH_3CH_2CH_2OH + 18OH^-$	−0.733

2.1.1 Electrocatalytic process

In general, an overall electrocatalytic process consists of cathodic and anodic processes occurring in two compartments separated by a membrane to prevent the mixing of the respective products, as shown in Fig.2.1. Over the course of the reaction, a non-spontaneous electron transfer is driven by an external power supply, to activate the reduction mechanism on one electrode (cathode), while the other (anode) oxidizes [24]. So, the conversion of the reactants occurs at the cathode together with the competing HER, while the oxygen evolution reaction (OER) commonly occurs at the anode thereby providing the necessary protons and electrons. The charge transfer between electrodes (electron-conducting phases) occurs within an electrolyte medium (ion-conducting phase), while the electrochemical reduction of the reactants takes place at the cathode electrode/electrolyte interface. As a rule, the CO_2RR involves three major steps [25]:

1. Mass transport of CO_2 molecules to the catalyst layer and chemical adsorption onto its surface. This process weakens the linear structure and lowers the energy barrier for the following reactions.

2. The activated CO_2 species are reduced through sequential transfer of electrons and protons, which leads to the formation of reaction intermediates.

3. The fully reduced reaction intermediates undergo rearrangement into final products and subsequently desorb from the catalyst surface.

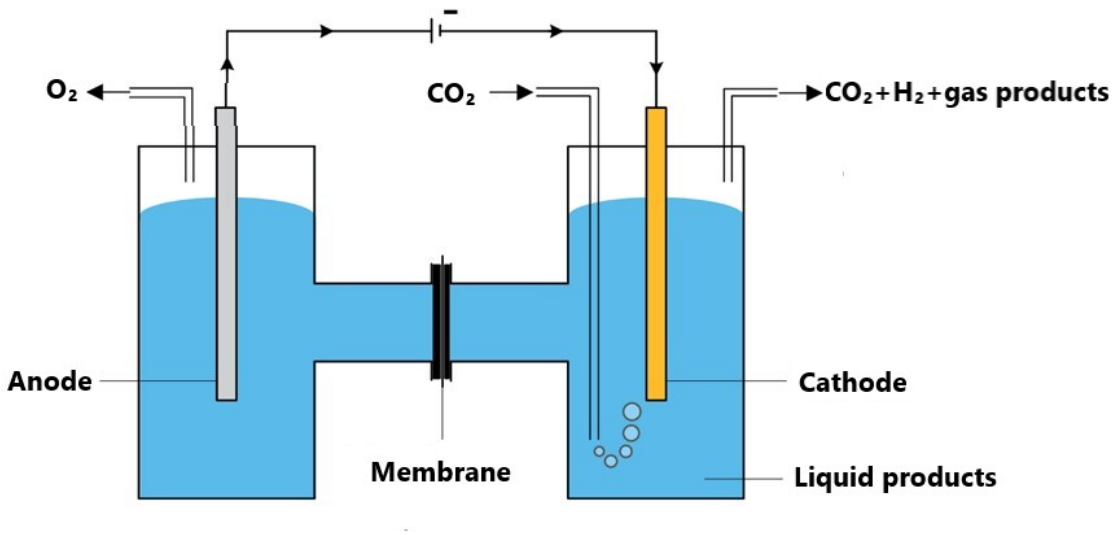

Figure 2.1: Schematic representation of a conventional electrocatalytic system for the CO_2RR [26].

2.1.2 Electric double layer

In electrochemistry the electrodes are affected by the negative charges present on their surface, which in turn influence their interaction with the electrolyte, and lead to the formation of a region called the electrical double layer. The structure of the electrode/-electrolyte interface is typically divided into five distinct regions, namely the electrode surface, the inner Helmholtz layer (IHL), the outer Helmholtz layer (OHL), the diffuse layer and the bulk solution [27] (see Fig.2.2). The closest layer to the working electrode is the IHL, which contains the adsorbed reactants and the reaction intermediates, while the OHL is comprised of solvated ions with the opposite charge of that of the active electrode. The diffuse layer contains non-specifically adsorbed ions and together with the Helmholtz layer form the electrical double layer [28].

Overall, its conformation affects the local reaction environment by modifying the interfacial electric field and ion distribution, thereby impacting the kinetics and selectivity of the CO_2RR. Usually, the conversion of CO_2 is an inner-sphere process because the adsorption and bond rearrangement of its molecules and reaction intermediates proceed within the IHL [29],[30]. So, an improved understanding of the electric double layer highlights the critical role of electrode morphology and surface structure in steering product selectivity during the CO_2RR. The choice of the catalyst material is only the first step as it needs to be nanostructured for enhanced performance, since certain sites at catalytic surfaces are usually inactive because of their inability to stabilize adsorbates and reaction intermediates [31].

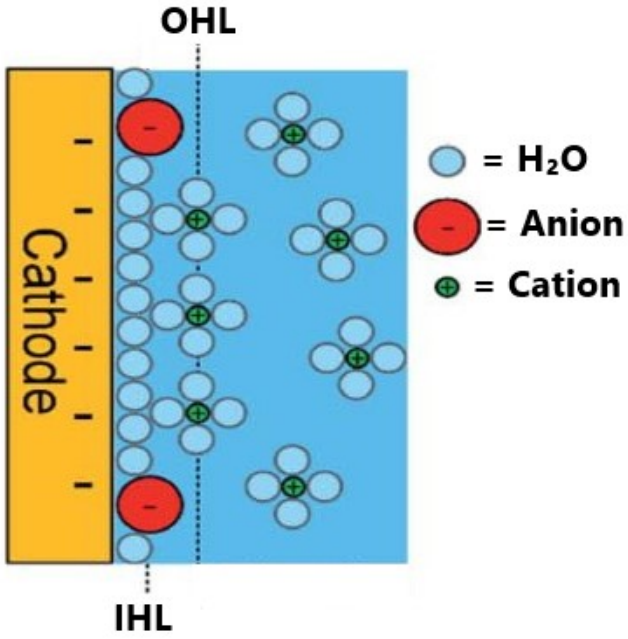

Figure 2.2: Visual overview of the electrochemical double layer with specifically adsorbed anions at the IHL and solvated cations at OHL [26].

2.1.3 Electrolyte selection

The choice of electrolytes also plays a fundamental role in determining the efficiency and selectivity of the CO_2RR, as it significantly influences the structure of the electric double layer. The solvated metal cations at the OHL can electrostatically interact with adsorbed species and influence the distribution of products [32]. In general, the electrolyte provides ionic conductivity and charge balance between anodic and cathodic reactions. Moreover, it should not interact with the electrode materials thereby ensuring a stable pH environment, which is essential for maintaining reaction kinetics and product selectivity.

Since carbonates are chemically compatible with most electrode materials, they are commonly employed in aqueous systems [33]. In addition, bicarbonate solutions, such as potassium bicarbonate ($KHCO_3$, 0.1-1M), provide capacity to buffer the local pH at the electrode surface during the reduction of CO_2 [34], thus maintaining a stable environment and homogeneous reaction conditions due to the consistent proton availability. Neutral and slightly alkaline electrolytes are therefore widely used, since acidic environments strongly promote the competing HER because of the abundance of protons, while highly alkaline environments induce the formation of carbonate and bicarbonate salts at the interface [35]. For these reasons, a careful selection of the electrolyte is essential, as it must be aligned with the choice of the catalyst and plays a critical role in governing interfacial interaction dynamics during the CO_2RR.

2.1.4 Reaction parameters

To perform a qualitative and quantitative evaluation and comparison of catalysts and devices employed for the CO_2RR, several key parameters are typically considered:

1. FE is defined as the ratio of the charge used to form a specific product, calculated from Faraday's law, to the total charge supplied for the overall reaction [36]. It is typically expressed as a percentage and indicates the fraction of electrons that contribute to the formation of the desired products.

2. Current density, that is the total current per unit area (mA/cm^2) of the working electrode and constitute the most direct measure of catalytic activity (rate of charge transfer) [37]. Together with the FE, it allows the evaluation of the catalyst products selectivity.

3. Energy efficiency, known as the percentage of energy stored in chemical products compared to the total electrical energy input that is proportional to the total cell voltage, as shown in Fig.2.3. Therefore, increasing energy efficiency means decreasing total cell voltage. The latter involves the thermodynamic cell voltage, defined as difference between the thermodynamic potentials of the cathodic and anodic reactions, the activation voltage drop at a specific current density, and the ohmic voltage drop, caused by current flow resistance in electrode, electrolyte and membrane [38].

4. Stability, defined as the ability of the catalyst system to maintain its performance over time (long-term durability) under continuous operation. It is a critical parameter for scaling CO_2RR technologies to industrial applications.

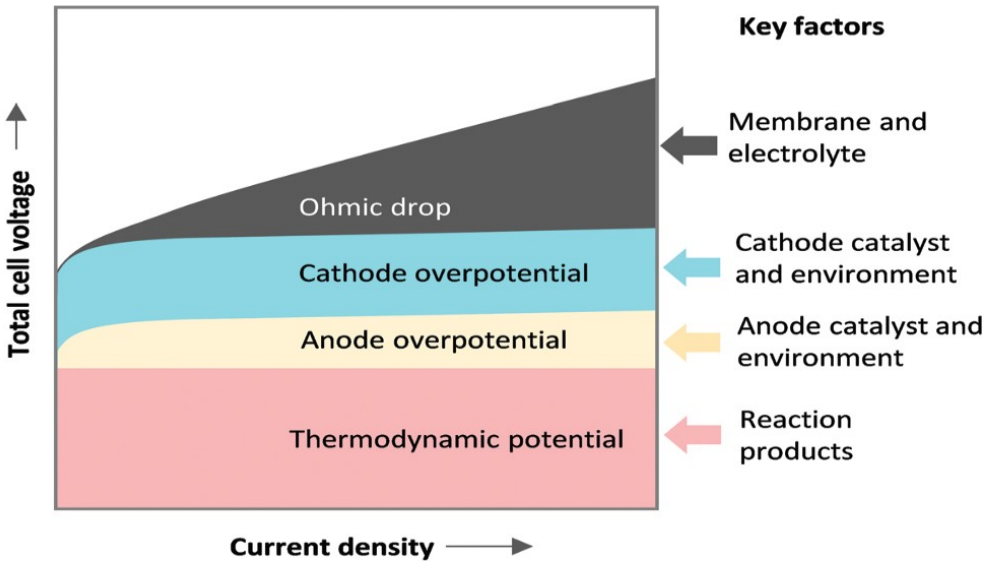

Figure 2.3: Total cell voltage components as a function of current density [38].

2.2 Catalyst materials

The choice of the catalyst is the most crucial factor in determining the activity, selectivity and efficiency of the CO_2RR. Since this process involves multiple competing reaction pathways, the reaction outcome is ultimately determined by each material capability of binding with the key intermediates [39].

2.2.1 Copper

Cu-based materials are the most widely studied group metal catalysts that allow room-temperature reduction of CO_2 into highly reduced multi-carbon products with relatively high energy efficiencies [40],[41]. As a rule, Cu is the only known metal that can selectively catalyze the formation of products requiring more than two electron transfer steps [42],[43], due to its unique ability to stabilize the reaction intermediates, which can then be further reduced [44]. Those are usually called C_{2+} products and include ethylene (C_2H_4), ethane (C_2H_6) and ethanol (CH_3CH_2OH), which are all high-valuable chemicals and energy-dense fuels. The reason is that Cu has strong enough binding energy to stabilize *COOH, *CO and *CHO intermediates, preventing their immediate desorption without leading to irreversible adsorption and thus surface poisoning, which is beneficial for further C-C coupling and forming multi-carbon species [45],[46]. Therefore, depending on the system configuration, which includes the electrode design, electrolyte choice and cell setup, specific reaction pathways are favored (see Fig.2.4), ultimately determining the distribution of products [47],[48]. However, Cu typically produces a broad spectrum of products with low selectivity, thus requiring energy-intensive separation processes [49].

Moreover, its activity tends to degrade during operation due to the CO_2RR products, which can lead to surface restructuring, and partial dissolution under reaction conditions, thereby hindering long-term stability [50]. A major limitation of Cu-based materials is their significant HER activity, which competes with the CO_2RR and lowers overall conversion efficiency [51]. Since the morphology and the crystallite size of the Cu electrocatalysts are key factors influencing CO_2 conversion performance [52], they must be understood and carefully optimized.

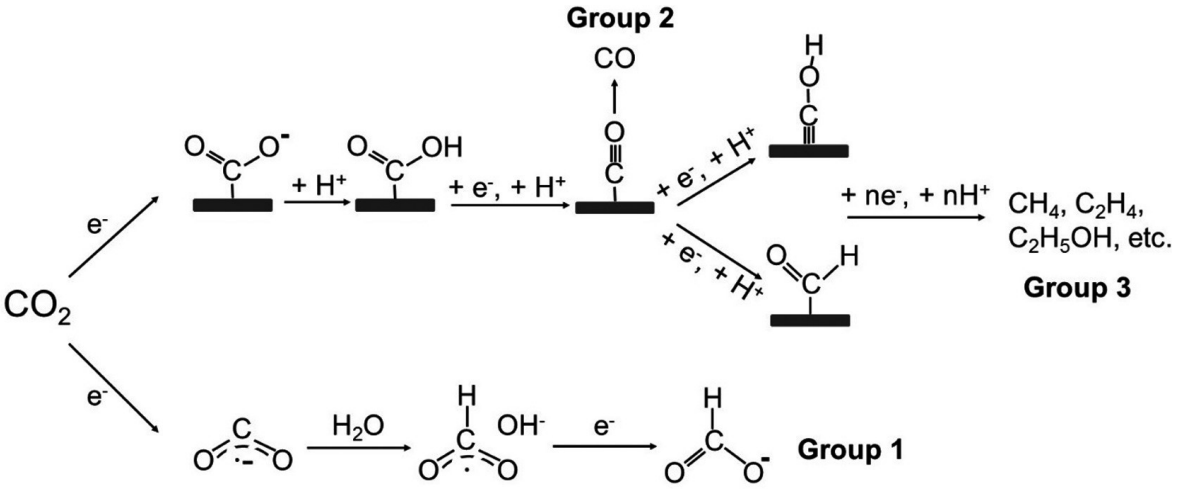

Figure 2.4: Possible mechanism of the CO_2RR in aqueous systems [25].

2.2.2 Noble metals

Noble metals, in contrast, show a narrower selectivity window at lower overpotential with respect to Cu. Specifically, silver (Ag) and gold (Au) are highly effective in converting CO_2 to CO with excellent FE [53],[54]. Despite Au offering exceptional stability, its high cost hinders large-scale applications, so Ag is usually preferred due to its greater natural abundance and lower material expense [55]. In addition, Ag has a significant lower hydrogen binding energy compared to Cu, so its presence near Cu-based catalysts results in a lower *H ions surface coverage under reaction conditions and therefore suppressed rates of HER [56]. For these reasons, coupling Ag and Cu to produce bimetallic catalysts offers a potential way to enhance the CO_2RR performance [57]. For example, the addition of Ag to Cu-based materials has been demonstrated to be an effective strategy for steering product selectivity toward C_{2+} oxygenates [58],[59]. This effect has been attributed to a cascade mechanism, called "tandem effect", which integrates two consecutive steps of CO_2-to-CO and CO-to-C_{2+} conversion on two distinct catalytic sites, thereby combining the different properties of each material [60].

Apart from noble metals, alternative elements such as antimony (Sb) are increasingly attracting attention as a cheaper yet promising alternative to promote the cascade mechanism in bimetallic catalysts [61]. Therefore, understanding the interactions between different materials within bimetallic electrocatalysts constitutes another key research priority for improving the CO_2RR.

2.3 Bimetallic electrodes

The development of bimetallic electrodes has emerged as an effective strategy to improve the performance of the CO_2RR beyond what is achievable with pure metals. Combining two different catalytic surfaces and thereby breaking down the multistep CO_2 conversion process into two consecutive steps, might be a strategy to overcome fundamental efficiency limitations and steer the selectivity toward fewer desired products [62]. A series of alloy materials including Au-Cu, Sb-Cu and Ag-Cu have been demonstrated for high efficiency C_1 products formation by stabilizing the critical intermediates [63],[64]. Meanwhile, various Cu-Ag catalysts have been reported to exhibit enhanced CO_2RR selectivity and activity toward multi-carbon products. The enhancement has been attributed to the suppression of the competing HER and thereby increased surface population of *CO intermediates on the catalysts [65],[66]. On one hand, the introduction of alloying element brings about change of electronic structure owing to charge transfer between matrix and the solute atoms, which further alters, to modulate binding strength of intermediates [67]. On the other hand, the addition of foreign atoms accompanies variation of atomic configuration in comparison with the monometallic counterpart, which plays a vital influence on the adsorption of intermediates at the active sites [68]. Generally speaking, the mechanism by which CO produced on Ag (or Au) sites diffuses toward adjacent Cu sites for further reduction into C_1-C_3 products [69],[70], as shown in Fig.2.5, is called "tandem effect" or "CO spillover" and can be employed to improve the CO_2RR performance. Moreover, the bimetallic electrode architecture can be designed in several forms, including alloyed nanoparticles, layered thin films, core-shell structures and spatially separated domains. Each one provides different degrees of interaction between the constituent elements, which in turn influence CO availability and reaction intermediates stabilization. For example, Ag nanoparticles-decorated Cu_2O nanocubes displayed enhanced selectivity toward C_{2+} liquid products, while the production of formate (HCOO-) and H_2 was suppressed. Most importantly, an increase in the size of Cu/Ag interfaces correlates with a stronger selectivity enhancement [71]. Despite these promising features, bimetallic electrodes still face limitations with respect to precise control of surface composition, scalability and long-term stability, which hinder the transition toward industrial implementation.

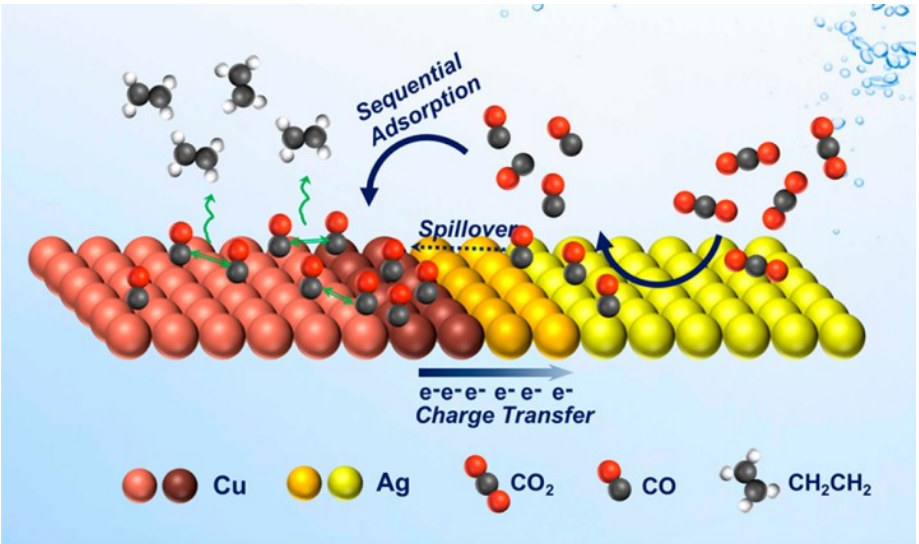

Figure 2.5: Schematic representation of the CO spillover mechanism in Cu-Ag bimetallic electrodes [72].

2.4 Electrode design

Besides catalyst composition, the architecture of the electrodes plays a central role in determining the CO_2RR performance. While the choice of the catalyst dictates the intrinsic activity and selectivity of the CO_2 conversion process, electrode structure governs the efficiency of reactants transport to the active sites and subsequent product removal. Specifically, it must enable efficient CO_2 delivery to the catalyst surface, minimize ohmic resistance, and ultimately enhance reaction kinetics [26]. One of the main limitations concerns mass transport, because the solubility of CO_2 in aqueous systems is relatively low at room temperature. This restricts reactants availability at the catalyst surface during electrochemical reduction, thereby constraining the reaction kinetics [73]. To address this issue, replacing liquid-fed electrodes with gas-fed counterparts represents a promising strategy, since the mass transport of CO_2 and reaction products can be enhanced by tuning the electrode architecture at the micro- and nanometer scale [74]. For these reasons, GDLs are often employed to support the electrodes, as they provide mechanical stability, high conductivity and a porous structure that facilitate CO_2 gas diffusion [75]. They are composed of a macroporous layer, the structural backbone that provides mechanical stability and high gas permeability, combined with a microporous layer (MPL) [76]. The MPL is hydrophobic and characterized by small pores composed of carbon powder and PTFE to prevent liquid electrolyte from seeping into the gas flow channel, while ensuring good electrical contact with the catalyst layer, thus minimizing ohmic losses at the interface [77].

Normally, GDLs are coupled with the catalyst layer to form GDEs, enabling high current densities and improved catalytic efficiencies when implemented in a flow cell or zero-gap cell [78]. Since CO2 gas can diffuse through the GDL to reach the electrode/electrolyte interface within the catalyst layer (see Fig.2.6), mass transfer limitations associated with sluggish kinetics are mitigated, thereby enhancing CO_2RR rates. Additionally, catalyst particles can be integrated into the porous structure using electrodeposition technique, providing a high active surface area. Carbon paper is widely used as substrates for GDEs, as it offers high electric conductivity, good mechanical stability, and an ideal hydrophobic porous structure, making it an excellent support for the CO_2RR.

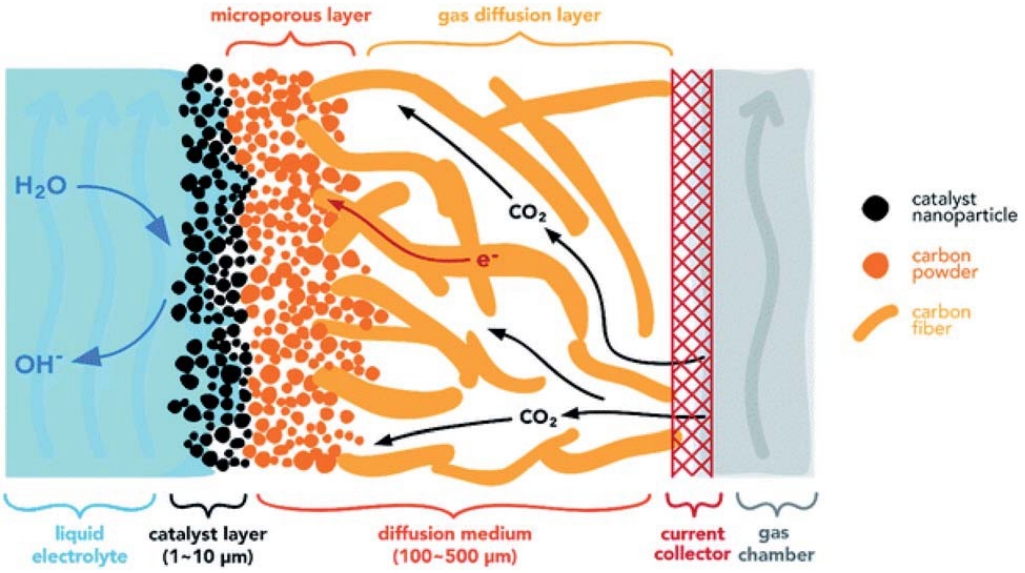

Figure 2.6: Visual overview of CO_2 diffusing inside the GDE structure [26].

2.5 Cell configuration

The configuration of the electrochemical cell is another key factor in determining the performance and reliability of the CO_2RR, since the overall efficiency of the process is also governed by how the electrodes, electrolyte and membranes are arranged within the reaction environment. Over the years, several cell designs have been developed, each with its own specific advantages and limitations:

1. The most traditional setup used in early research is the H-cell, which is comprised of independent cathode and anode chambers that are connected by an ion-exchange membrane [79], with the electrodes simply immersed in liquid electrolytes with CO_2 gas bubbled to saturate the catholyte.

While the cathode reduces CO_2, the anode typically oxidizes water to oxygen, following the OER. This configuration is simple, low cost, and allows rapid screening of novel electrocatalyst, but is not practical for large-scale deployments because the rates of CO_2 mass transfer to the electrodes surface are too slow and the achievable current density too low, thus preventing any industrial applications [80].

2. Flow cells were developed to overcome these limitations. In this setup, the cathode is a GDE where gaseous CO_2 is continuously fed to the catalyst layer, while the electrolyte is circulated in separate liquid channels, as shown in Fig.2.7. This design ensures a constant supply of CO_2, drastically the reaction kinetics and current density [81]. However, the presence of liquid electrolytes in direct contact with the GDE can lead to electrode flooding and carbonate precipitations, thus posing severe long-term stability issues.

3. Finally, the MEA configuration was developed, where the catalyst layer is directly integrated with (pressed against) the ion-exchange membrane (zero-gap design), so that the cathode/anode distance is reduced to a few micrometers thereby reducing the ohmic resistance. In addition, since the MEA configuration eliminates the presence of liquid electrolyte between the cathode and membrane, it prevents the flooding mechanism and limits the carbonate precipitations, while enabling even higher current densities [12].

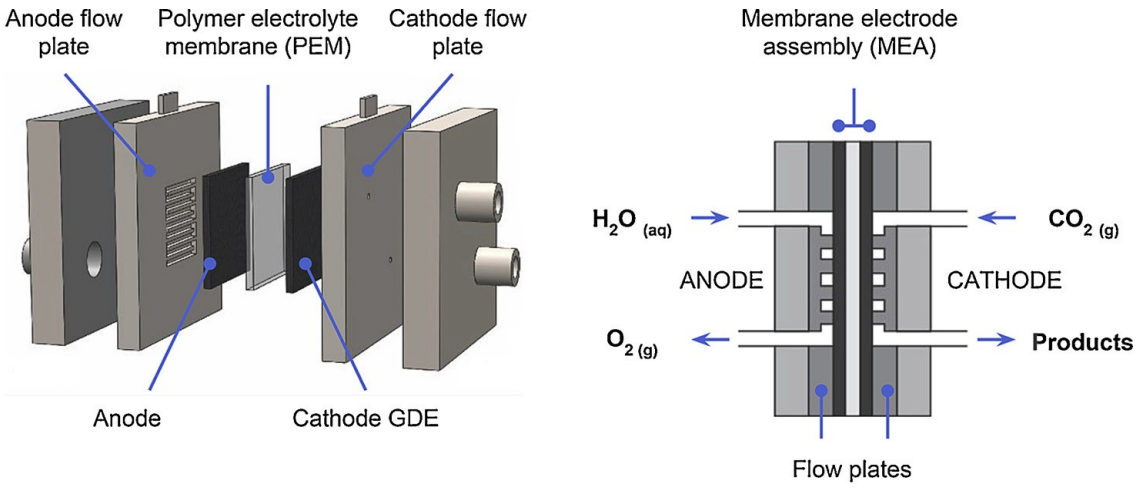

Figure 2.7: Simplified illustration of the flow cell configuration together with the MEA development [12].

It is also important to consider the role of the cathode/anode separators, specifically the ion-exchange membranes. They represent a critical component of the system, as they ensure efficient cell operation by preventing the exchange of reactants and products between the chambers (product crossover), minimizing the risk of short circuit between electrodes and providing mechanical support while preserving ionic conductivity [26]. There exist three main groups of membranes (see Fig.2.8):

1. Cation exchange membranes (CEMs), which are composed of polymer matrices functionalized with negatively charged groups that allow selective passage of cations from the anode to the cathode, while blocking anions and neutral molecules. However, in acidic environments they favor the competing HER.

2. Anion exchange membranes (AEMs) can transport hydroxide (OH^-) anions through positively charged functional groups, thus creating a locally alkaline environment at the cathode, while suppressing the HER. Commonly employed in MEA systems, they suffer from carbonate formation at the surface, which reduces the mass transport efficiency.

3. Bipolar membranes (BMPs) combine both PEM and AEM layers within a single structure. Water dissociation occurs inside the junction, allowing the simultaneous supply of H^+ and OH^- depending on polarization, thereby generating a pH gradient across the membrane.

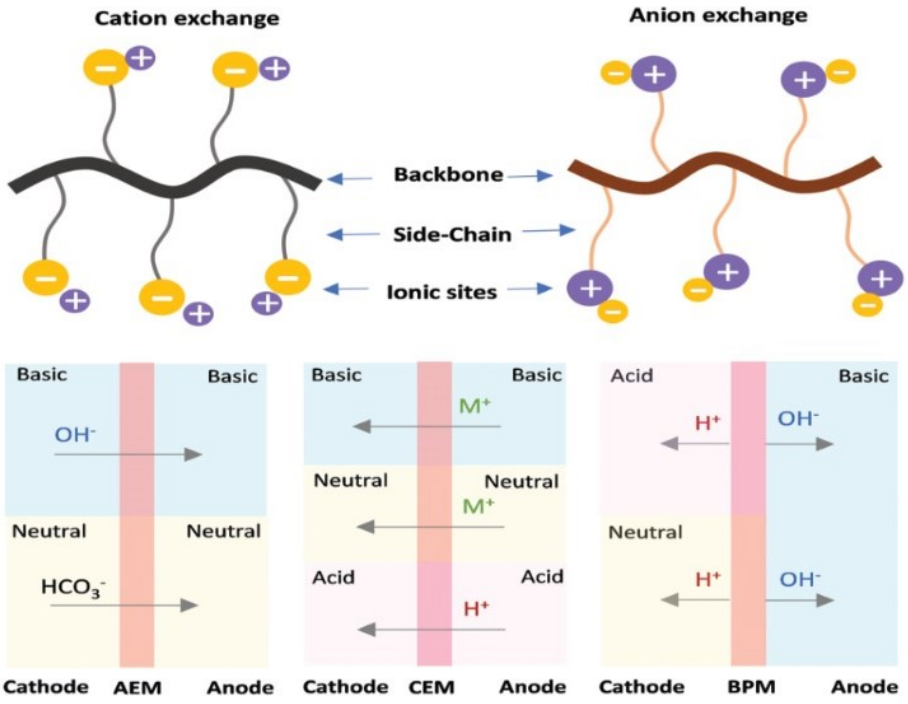

Figure 2.8: Graphical summary of the existing ion-exchange membrane properties [38].

CHAPTER 3

Materials and methods

This chapter describes the experimental procedures and analytical techniques employed in this work. It outlines the preparation of the GDEs, including Cu electrodeposition and Ag displacement, followed by the physical and electrochemical characterization of the samples. Furthermore, the analytical methods used to evaluate the selectivity of gaseous and liquid products are presented.

3.1 Electrodeposition process

Electrodeposition is a versatile and cost-effective technique used to fabricate metallic coating and nanostructured films on conductive substrates. In the context of the CO_2RR, Cu electrodeposition on carbon-based substrates allows precise control over the catalyst loading, particle size and surface morphology, all of which strongly influence catalytic performance and product selectivity. This process involves the reduction of Cu ions, present in a liquid electrolyte, onto the surface of a conductive substrate under the influence of an applied potential or current, leading to controlled growth of a metallic layer. Normally, the electrodeposition method is governed by the reaction conditions:

1. The composition of the electrolyte, which plays a major role, because the concentration and nature of the metal precursors strongly influence the nucleation and growth rates of the catalyst layer, due to their specific mass transport properties and availability during the reduction process.

2. The applied potential or current density, otherwise known as the driving forces of the reduction mechanism, that determine the sample morphology and the mass loading on the substrate for a given time.

3. The deposition time, which is the total duration of the reduction process on the target and dictates the overall thickness of the metallic layer at a given potential/current.

Generally speaking, electrodeposition is attractive for catalyst preparation because it combines simplicity (easy setup), reproducibility and cost-effectiveness. Unlike other methods like sputtering or chemical vapor deposition, this procedure requires only an electrochemical cell, a metal salt solution and electrical power source, without the need of vacuum systems or high temperatures, while offering precise control over surface morphology by tuning the deposition parameters.

3.2 Electrode preparation

3.2.1 Copper electrodeposition on carbon paper

In this thesis work, Cu electrodeposition was performed on commercial GDL carbon paper inside a two-electrode flow cell, to obtain free-standing GDEs. The chosen electrolyte was a solution of acetonitrile (CH_3CN, ACN) and copper acetate ($Cu(CH_3COO)_2$ anhydrous), 0.5g of $Cu(CH_3COO)_2$ was added into 100 ml of ACN in a glass beaker, followed by magnetic steering for half an hour to facilitate complete dissolution of the metal salts in the solvent. The choice of the solvent was determined by the need to ensure the full wettability of the hydrophobic GDL substrate, to guarantee the complete access of the electrolyte inside its porous structure and thereby homogenous and reproducible depositions. Regarding the setup of the flow cell, it is composed of individual gasket pieces properly cut and assembled together (see Fig.3.1), alternating the rigid and the soft ones (black and white ones), in such a way to obtain two connected chambers, but with different functions. The idea is to build two separate compartments, one between anode and cathode of approximately two millimeters, where the metal reduction can occur (working chamber), while the other, about double the thickness, is employed as a supply chamber to prevent the working chamber from emptying and thereby securing proper execution of the procedure for all its duration. This happens because ACN tends to evaporate at ambient temperature, that is the condition in which the electrodeposition was performed, thus emptying the working chamber during the course of the process. Prior to this development, the electrodepositions inevitably faced failure in obtaining homogeneous catalyst layers. Since the flow cell was positioned with the anode below the cathode, the supply chamber was placed above the cathode, so that gravitational force maintained the working chamber in a constantly filled state, as the upper one emptied. With this configuration, a total of approximately twenty milliliters of electrolyte was required for each deposition process. A thin Cu plate was chosen for the anode, to be used as reference electrode and provide an extra supply of Cu ions, since those dissolved in the small amount of electrolyte employed were not sufficient to guarantee the entire duration of the electrodeposition.

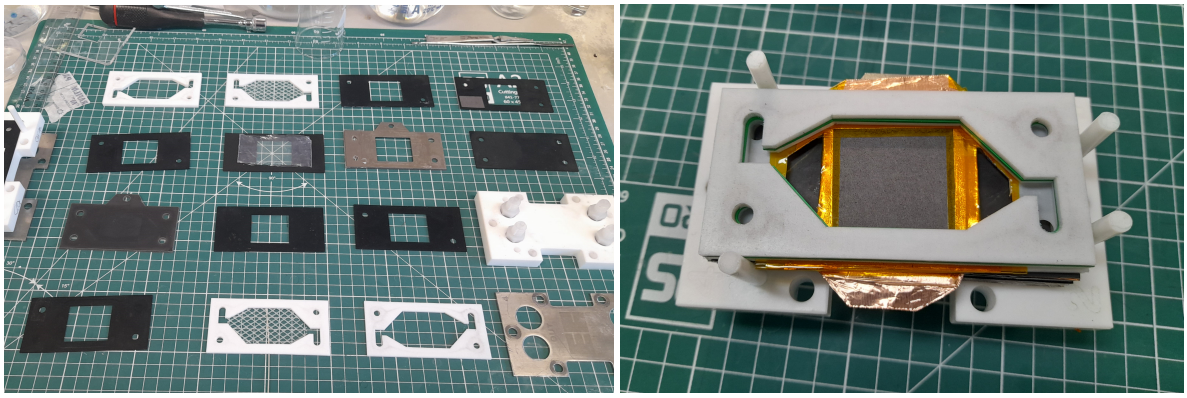

(a) Gasket pieces (b) Double chamber

Figure 3.1: Cell assembly from individual components.

However, it needed a clean procedure after each use, because each deposition process led to the formation of an oxide layer that prevented subsequent uses. The cleaning was performed inside a suction hood with hydrochloric acid (HCl, 2M), directly pouring on the oxidized anode. The cathode preparation was more complex, since it required the manual assembly of the GDL carbon paper on a gasket support, one of the soft pieces which were part of the flow cell. First, the carbon paper was cut to specific measures (shown in Fig.3.2), to fit inside the working chamber while still offering both a great surface area ($9cm^2$) and enough space for the electrical contacts, necessary for the connection with the external circuit. Then, it was meticulously cleaned with acetone to prevent most of the contamination from sticking to its surface and thereby entering the hermetic chamber, thus altering the deposition process with the presence of unwanted elements.

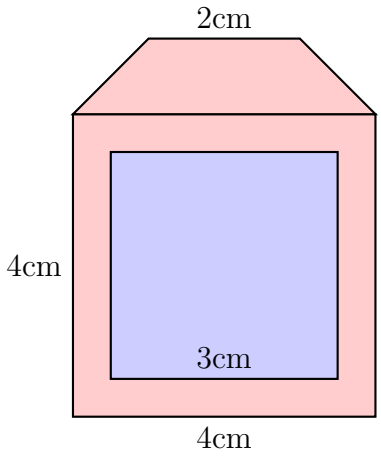

Figure 3.2: Visual representation of the sample dimensions: in blue the carbon paper active area, in red the conductive Cu frame.

Afterwards, using appropriate tapes, a conductive Cu frame was applied with great precision around the entire perimeter and both sides of the carbon paper to ensure homogeneous electrical contacts, which result in a smooth electric potential distribution all around the target. In addition, above the Cu tape an insulator one, made of polyimide (Kapton), was then applied. The latter one is essential to prevent the electrolyte from reacting with the conductive frame, thus altering the local environment of the cathode surface during electrodeposition and preventing repeatable results from being accomplished. After the completion of these preparations, the flow cell was finally assembled and filled with electrolyte using appropriate syringes. Although a flow cell setup was used, it was operated without active flow to ensure a more uniform mass transport environment, since the first depositions, performed with fluxing electrolyte, were found to be uneven and useless to replicate. This was accomplished by closing two of the four entrances with syringes, one empty and one full of electrolyte, while the other two were already closed because of the way the component pieces of the cell were cut and assembled (see Fig.3.3). The filling of the cell has been the most complex part, since it led several times to leakage issues, maybe due to the extra pressure applied inside the chambers during the procedure, and required careful handling. However, it never compromised critically the conduct of the electrodeposition, since the leaks would have eventually stopped after a few minutes. Moreover, to ensure full wetting of the highly porous carbon paper, the system was left at rest for several hours both before the initiation and after the completion of the deposition process, while monitoring with an open-circuit voltage technique (OCV), to obtain a stable potential between the electrodes.

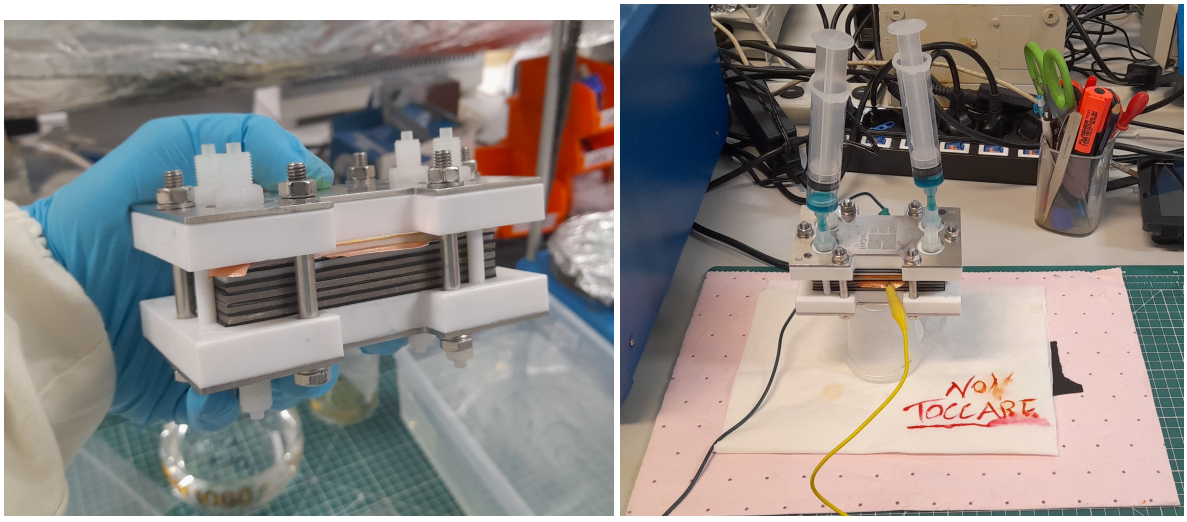

(a) Complete assembly (b) Electrical contacts

Figure 3.3: Real laboratory cell setup.

This step was necessary for measuring electrical resistance with a potentiostatic electrochemical impedance spectroscopy (PEIS). The latter one is particularly informative, as a decrease in electrode resistance is expected following the deposition, due to the higher electrical conductivity of Cu with respect to carbon paper, thereby confirming the proper occurrence of the process. Finally, the electrodeposition was performed by applying a constant negative potential to the cathode using a chronoamperometry (CA), with values ranging from -300 mV to -500 mV, for a given time. This potential range was selected following a cyclic voltammetry (CV), a technique in which the potential is cycled linearly between two values while the resulting current is recorded, thus providing informations on the redox processes [82]. A series of experiments were performed at 50 mV increments across the selected potential range, with a deposition time of both four and eight hours, in order to gain full knowledge of the procedure and select the most uniform catalysts for the electrochemical characterization with CO_2. Additionally, Cu mass loading on the substrate was estimated through weighing the sample before and after the deposition using an analytical balance. These measurements, together with the material characterization, enabled the comparison of all the GDEs prepared under different process parameters. It is important to clarify that the experimental setup did not include a reference electrode, since it led to unsolvable leakage problems. Therefore, the applied potential refers to the voltage directly imposed between the anode and the cathode, with the cathode held at a negative potential relative to the anode to enable metal deposition.

3.2.2 Silver galvanic displacement

Once the Cu deposition process had occurred, the fabricated samples were manually cut from their frames before proceeding to the next step. The method involving the formation of bimetallic catalysts is known as galvanic displacement. This mechanism relies on the difference in standard reduction potentials between two metals. When a Cu-coated substrate is immersed in a solution containing Ag ions, a spontaneous redox reaction occurs because Ag has a higher reduction potential than Cu. This process results in the partial replacement of the outermost Cu atoms by Ag atoms, forming a surface enriched Ag layer while maintaining the underlying Cu structure [83]. Moreover, it does not require an external power source, because the redox reaction proceeds spontaneously. This procedure was performed by immersing the Cu-based electrodes in a suitably heated aqueous solution of silver sulfate (Ag_2SO_4, 0.5mM) for a few minutes, so that the heat could enhance the reaction kinetics. The Ag solution, placed in a small glass beaker, was brought to temperature (70°C) through a bain-marie inside a silicon oil heated on a hotplate, as shown in Fig.3.4. After approximately five minutes, the electrodes were carefully removed using tweezers and dried under a gentle stream of nitrogen gas, taking care to avoid altering their morphology due to excessive flow.

This method allowed the simple fabrication of bimetallic GDEs, which will be further characterized to understand their physical and chemical properties and compare them with the monometallic ones.

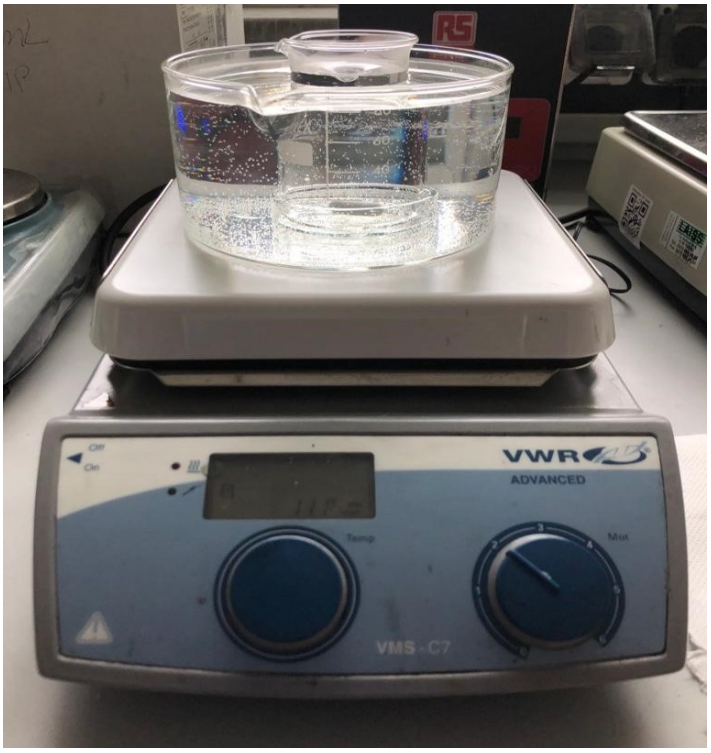

Figure 3.4: Real setup of Ag displacement.

3.3 Material characterization

A comprehensive understanding of the morphology and composition of the synthesized GDEs is essential to establish reliable correlations with physicochemical properties and electrochemical performance. Moreover, such studies unveil the correlation between electrodeposition process parameters and the resulting samples conformation, which in turn affects the CO_2RR. For this purpose, a combination of mutually informative techniques was employed, namely FESEM and EDS. These studies provided information about the surface morphology and the chemical composition of the samples, respectively.

3.3.1 Field Emission Scanning Electron Microscopy

FESEM is a powerful technique used for imaging the surface of the electrodes with really high magnification (up to 10^6) at nanometer resolution. This analysis is essential to understand the effects of the different electrodeposition parameters on the morphology of the fabricated samples. FESEM employs a field emission gun to generate a highly focused electron beam with small probe size and high brightness, which is focused by two sets of magnetic lenses toward the target. The gun is composed of a sharp single-crystal tip, where a huge electrostatic field is generated by applied potential, so that the electrons could be extracted by the tunneling effect. Subsequently, the condenser lenses confine the electron flux while the objective lenses focus the beam on the samples surface to obtain optimal focal length. When the electron beam interacts with the surface atoms, various signals are generated, including backscattered electrons (BSE), secondary electrons (SE), Auger electrons and characteristic X-rays (see Fig.3.5). SE are low-energy electron ejected from the very surface layers of the sample and provide high-resolution images of the surface morphology with excellent sensitivity, while BSE are higher-energy electrons that are reflected back from deeper regions of the sample and thereby offer higher depth of field and compositional contrast between light and heavy elements. The combined detection of these signals enables the acquisition of detailed topographical images, while preserving high depth of field, of the material surface, effectively highlighting particle size distribution and uniformity of surface coverage of the analyzed samples.

3.3.2 Energy Dispersive Spectroscopy

EDS is an analytical technique coupled with FESEM system to determine the elemental composition of a sample. This method has been essential to confirm the presence of Ag on Cu-based samples fabricated with the displacement procedure. EDS collects and analyzes characteristic X-rays, unique to each element, which are emitted by the electrode atoms as a result of electronic relaxation of their inner shell following the excitation caused by the impinging electron beam. Typically, the detector consists of an array of different p-i-n junctions cooled at cryogenic temperatures, so that electron-holes pairs are created when a specific X-ray comes at their surface, thus giving both qualitative and quantitative information of the elements present. By coupling EDS with mapping functions, the complete spatial distribution (two-dimensional map) of the various elements present on the sample is obtained.

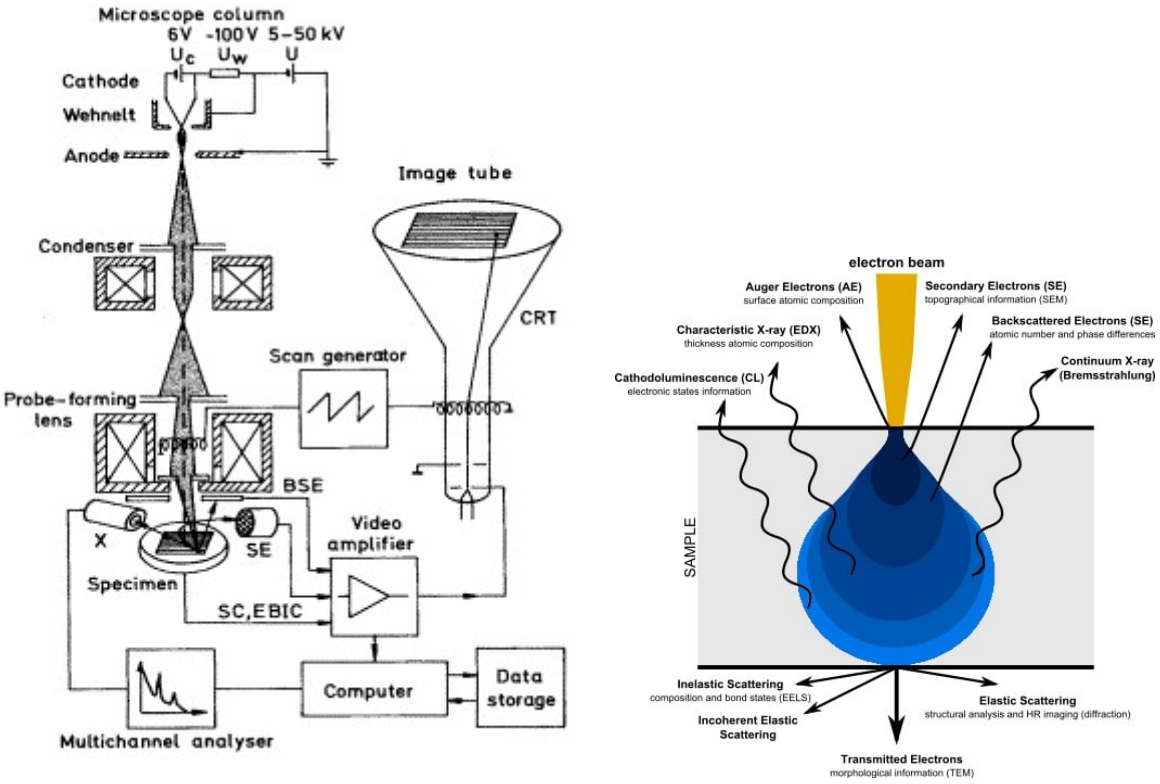

(a) Schematic illustration of FESEM. [1]

(b) Interaction area of the e-beam. [2]

Figure 3.5: Working mechanism of a FESEM device.

3.4 Electrochemical characterization

The electrochemical characterization was performed mainly through a series of galvanostatic and potentiostatic tests, with the MEA configuration chosen as reaction environment, where the CO_2RR has been driven at a fixed current density while monitoring the resulting cell potential over time.

3.4.1 MEA cell configuration

Electrochemical measurements were carried out using a MEA cell configuration. In this setup, the cathode (working electrode) is chosen from the previously fabricated Cu-based or bimetallic GDEs, while the anode is an iridium-coated titanium mesh (IrO_2-Ti), selected for its high stability toward the OER.

[1] https://inano.au.dk/research/research-platforms/nanoanalysis/transmission-and-scanning-electron-microscopy

[2] https://atriainnovation.com/en/blog/scanning-electron-microscopy-uses/

For each test, the fabricated GDEs has been precisely cut from the frames before utilization (2.23cm x 2.23cm), since a defined area of 5cm^2 was required to accurately evaluate the current density applied during subsequent galvanostatic tests. The remaining part was then stored for the upcoming material characterization. Both the electrodes were pressed directly against the ion-exchange membrane, to minimize the ionic resistance. The latter one has been previously activated and stored inside the electrolyte used for the measurements, which is potassium bicarbonate ($KHCO_3$, 0.1M), to prevent it from drying out. However, the concentration of the electrolyte employed for the activation of the membranes was ten times higher than the one used for storage, to ensure that maximum conductivity was achieved prior to application. Finally, the cell was assembled and closed with a torque wrench, to guarantee that all sides exerted the same pressure inside of it, thus preventing any imbalance in the local reaction environment. The cathode side of the MEA was supplied with pure CO_2 gas at controlled flow rate of 25 ml/min, while the anode side was continuously fed with a recirculating $KHCO_3$ electrolyte at 10 ml/min. The gas outlet was connected to a micro-gas chromatograph (µGC, Fusion, INFICON) for the real-time analysis of the gaseous product selectivity, whereas the liquid outlet was connected back to the electrolyte reservoir to maintain continuous circulation throughout the measurement. In addition, a trap was installed along the gas line to prevent any liquid residues from entering the µGC by allowing their collection beforehand. Following these preparations steps, electrical contacts were applied to the MEA cell, to carry out the electrochemical analysis performed with the use of a CH potentiostat (CH1760D). Liquid samples were taken during the measurement to estimate the selectivity of the liquid products inside a high-performance liquid chromatograph (HPLC, Nexera series, SHIMADZU).

3.4.2 Electrochemical test: LSV, PEIS, CP

In this work, three complementary techniques were mainly employed:
linear sweep voltammetry (LSV), PEIS and chronopotentiometry (CP):

1. LSV consists in scanning the working electrode potential, in a range between 0 and 4 V, linearly with time while recording the resulting current response (see Fig.3.6a). This technique gives information about the minimum potential at which catalytic activity becomes evident, which usually occurred once 2.5 V was exceeded. In addition, it provides evidence of the electrochemical reduction of Cu oxide to metallic Cu during the procedure, since oxide-derived materials can lead to morphology or structure evolution during in situ reduction processes [84].

2. PEIS involves applying a small sinusoidal potential perturbation around a fixed potential and measuring the current response over a range of frequencies. The data are typically represented in a Nyquist plot and analyzed with equivalent circuit models to extract resistance values (see Fig.3.6b).

This technique is used to investigate the stability of the electrode/electrolyte interface and the efficiency of mass transport. When the estimated resistance exceeds a certain threshold, such as one ohm, the reaction kinetics could be hampered by poor cell closure or defective membranes.

3. CP, also known as current electrolysis, is a galvanostatic technique in which the current passing through the MEA cell is fixed, while the working electrode potential is continuously recorded as a function of time, as shown in Fig.3.6c. The CP represents the core of the CO_2RR analysis, because it simulates realistic electrolysis conditions, where the electrodes must sustain fixed current loads to drive the reduction of carbon dioxide into the different reaction products at a controlled rate. Meanwhile the time evolution of the potential provides insight into the stability of the catalytic system, as a sudden change of it typically reflects a system failure resulting from either catalyst degradation of GDE flooding. The measurements were performed at constant current of 1000 mA for a maximum of two hours. The total charge passed during this procedure has been utilized to compute the FEs of each product, both gaseous and liquid.

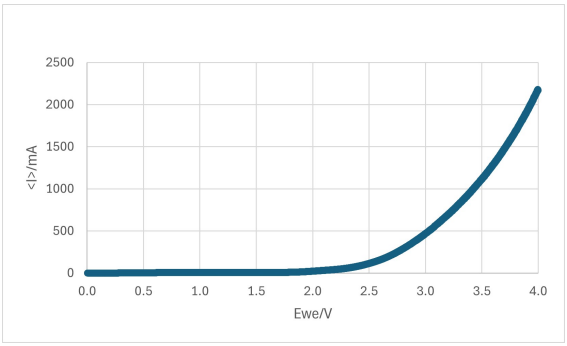

(a) Example of LSV

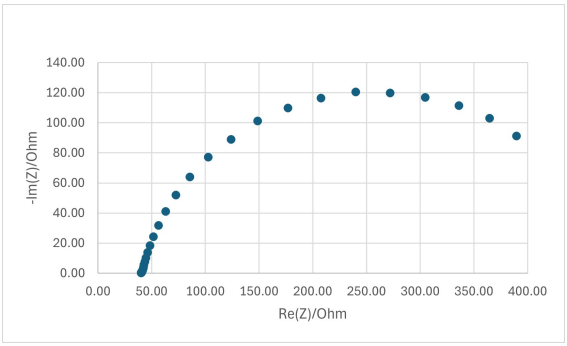

(b) Example of PEIS

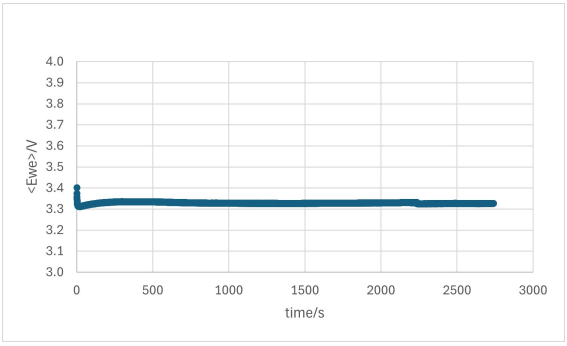

(c) Example of stable CP

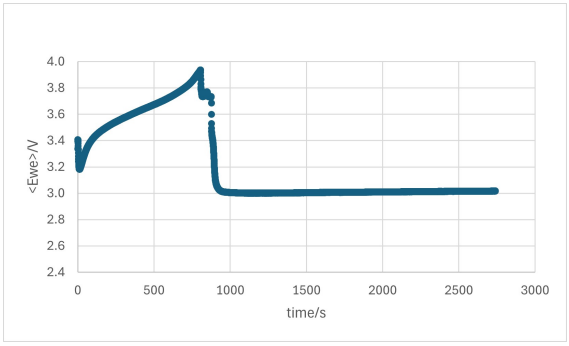

(d) Example of system failure

Figure 3.6: Examples of electrochemical measurements.

3.5 Product analysis

The accurate quantification of reaction products is essential to evaluate the selectivity of catalysts and compute the faradaic efficiency of each reaction pathway. In this work, two complementary chromatography techniques were employed to analyze both the liquid and the gaseous products.

3.5.1 Gas Chromatography

Gas chromatography is a widely used analytical technique to identify and quantify gaseous products formed during the CO_2RR. The recognition mechanism is based on the separation of volatile species in a gas stream (gas sample + mobile phase) as they pass through a chromatographic column (see Fig.3.7). In particular, our µGC system is composed of two columns: the first one uses argon as mobile phase (carrier gas) and deals with the separation of light molecules (CO, H_2, N_2, O_2), while the second one uses helium as carrier gas and deals with the separation of heavier gases (C_2H_4, C_2H_6). The instrument performs the online real-time analysis throughout the duration of the measure, since the effluent gas stream from the MEA cell is continuously directed inside the instrument. The gaseous samples are injected into a heated inlet, along with the mobile phase, where they are vaporized and subsequently carried into the columns that allow the separation of the different compounds. The detector identifies the difference in thermal conductivity between the reference (carrier gas) and the sample injected, generating an electric signal and leading to the chromatogram construction, which identifies the different gaseous species and displays their concentration. The instrument can reach 1 ppm (part per million) sensibility, which is very useful for identifying traces of products. However, calibration curves with standard gas mixtures are required to translate detector signals into molar concentrations and thereby compute the FEs of the sample with the following equation:

$$\%FE = \frac{\dot{V} \cdot C \cdot n \cdot F \cdot t}{V_m \cdot Q} \cdot 100 \tag{3.1}$$

where:

$< \dot{V} >$ is the flow rate of CO_2 at the cathode [L/min],

$< C >$ is the product concentration [%v/v],

$< n >$ is the number of electrons required for the reducing reaction,

$< F >$ represents the Faraday constant [96485.3 C/mol],

$< t >$ is the time interval (fixed at 1 min),

$< V_m >$ represents the molar volume for an ideal gas at standard conditions (0°C and 1 atm) [22.4 L/mol],

$< Q >$ is the total electric charge passing through the cell during 1 minute of measurement [C].

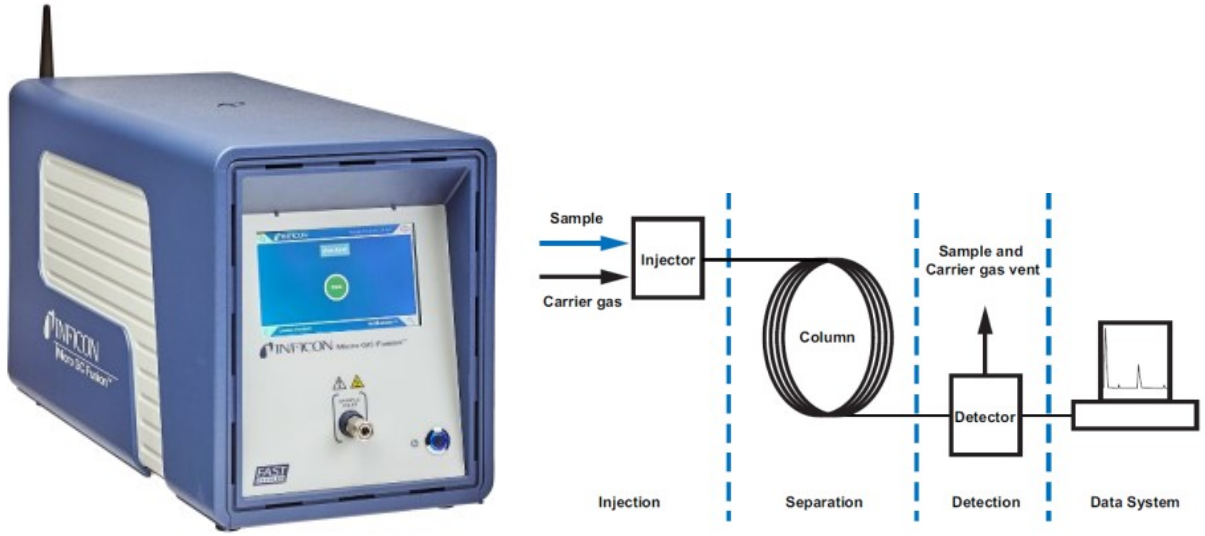

(a) GC device (b) Gas recognition mechanism

Figure 3.7: Gas chromatography technique

3.5.2 High-Performance Liquid Chromatography

The identification and quantification of liquid products formed during the CO_2RR is performed with liquid chromatography. Similarly to gas chromatography, the separation technique is based on the differential interaction of liquid samples carried by the mobile phase (sulfuric acid, 9mM) and the stationary phase packed inside the instrument (chromatographic column). Through this analysis, the retention time of the species found in the injected sample is displayed and thereby the individual components are identified. Meanwhile, the quantitative analysis is performed with a photodiode array detector (PDA) and a refractive index detector (RID), which function by exploiting the interaction of light with the analytes, such as absorbance and refractive index changes, as shown in Fig.3.8. Since each compound exhibits a unique electromagnetic absorption spectrum, the Lambert Beer's law (where the absorbance is directly proportional to the analyte concentration), can be applied to estimate the concentration of products. Specifically, our instrument includes two lamps, a deuterium (190-380 nm) one and a tungsten (380-800 nm) one, to cover all the UV/visible range.

The light emitted by the lamps irradiates the liquid sample contained in an optical cell, hence the transmitted light is both collected by the PDA to measure its absorbance and separated by a diffraction grating to detect the change in refraction index with the RID. The typical liquid products detected by the HPLC device are formic acid (HCOOH), acetic acid (CH_3COOH) and ethanol (CH_3CH_2OH). The quantification was carried out by calibration with standard solutions of target compounds, to enable the determination of product distribution and the calculation of the FEs, in conjunction with the total charge passed during electrolysis, with the followig equation:

$$\%FE = \frac{V \cdot C \cdot n \cdot F \cdot \rho}{MM \cdot Q} \cdot 100 \tag{3.2}$$

where:

$< V >$ is the sample volume [mL],

$< C >$ is the product concentration [%v/v],

$< n >$ is the number of electrons required for the reducing reaction,

$< F >$ represents the Faraday constant [96485.3 C/mol],

$< \rho >$ is the product density [g/mL],

$< MM >$ represents the product molecular weight [g/mol],

$< Q >$ is the total charge passed during electrolysis [C].

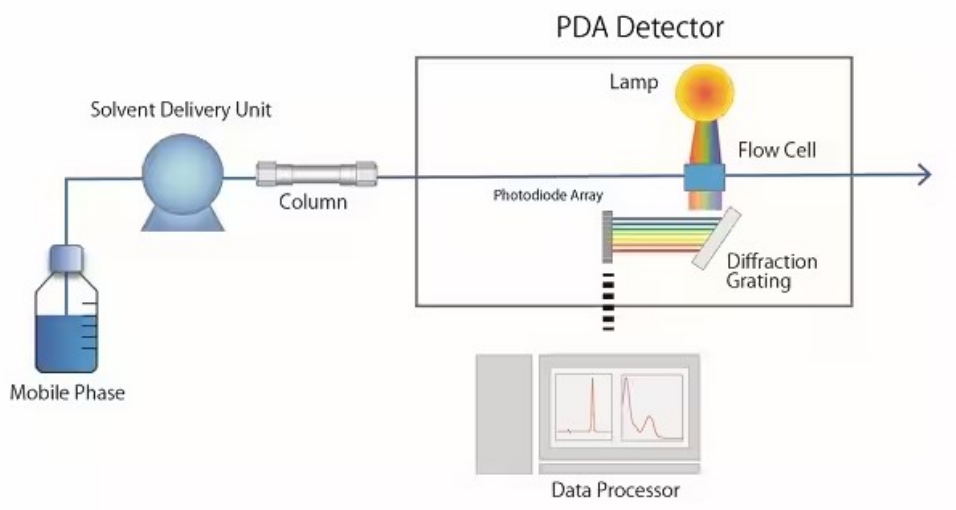

Figure 3.8: PDA mechanism

CHAPTER 4

Results and discussion

The performance of the CO_2RR strongly depends on a combination of structural, morphological and electrochemical properties of the catalysts. In this chapter, the results obtained from the preparation and characterization of Cu and Cu-Ag samples are presented and discussed. The Cu GDEs include: Cu300, Cu350, Cu400, Cu450, and Cu500. The number in the sample name indicates the electrodeposition potential without negative sign. E.g. Cu300 is the Cu electrode prepared at -300mV. Moreover, the Cu-Ag GDEs include Cu300-Ag and Cu400-Ag, indicating that the Cu substrates are Cu300 and Cu400 respectively. The analysis is organized into three main parts: first, the physical characterization of the fabricated GDEs, focusing on surface morphology, mass loading and electrical resistance; second, the evaluation of their electrochemical behavior in MEA cells through LSV, PEIS and CP; third, the analysis of product selectivity with GC and HPLC. The objective is to correlate structural features with electrochemical performance, thereby identifying the factors that most influence activity and reaction products selectivity for the CO_2RR.

4.1 Physical characterization

The study of physical properties enable a comparison between the GDEs obtained from the various deposition, thereby allowing an assessment of the experiment's reproducibility. After extensive preliminary testing, a fixed deposition time of 8 hours was selected. With the electrolyte composition held constant, the study proceeded by varying only the applied potential. In the following, the different properties of some of the best selected samples will be presented:

1. FESEM imaging offered valuable insights into the surface morphology, which plays a key role in governing the interaction between CO_2 and the catalytic material. The electrodeposition, performed on carbon paper (see Fig.4.1), produced a granular Cu layer uniformly distributed along the carbon fibers, characterized by excellent surface coverage, good roughness and high active surface area.

2. The total amount of catalyst deposited on the substrate, known as mass loading, also plays a critical role in determining the CO_2RR performance of the fabricated GDEs. An optimal mass loading ensures a sufficient density of active sites while maintaining the porosity of the carbon paper, which is necessary for efficient gas transport. Excessive loading often results in particle agglomeration and pore blocking, hindering CO_2 diffusion and reducing accessibility to catalytic sites. On the other hand, too little loading limits the overall activity due to the scarcity of active centers. The deposition procedure allowed precise control of Cu loading, by tuning the reaction parameters such as the applied voltage and the deposition time.

3. The electrical conductivity is another crucial parameter, as it influences charge transfer and overall cell efficiency. Bare carbon paper, while conductive, suffers from relatively high resistance due to its porous structure and limited conductive pathways. The resistance analysis of the GDEs after Cu deposition demonstrated that the process was successful, as evidenced by the significant decrease in electrical resistance, since the metallic coating provided continuous conductive channels along the carbon fibers.

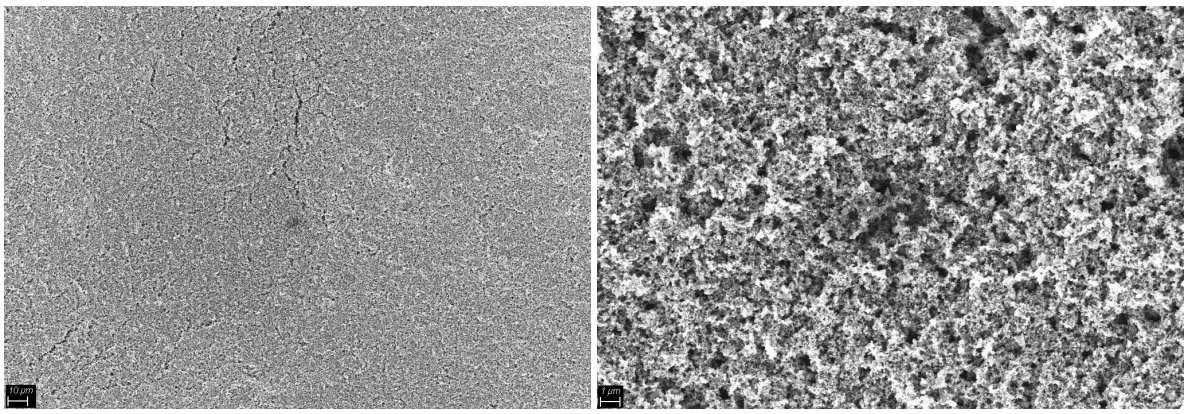

(a) FESEM at 1K magnification (b) FESEM at 10K magnification

Figure 4.1: FESEM performed on naked carbon paper.

4.1.1 Cu300 samples

The samples displayed in Fig.4.2 were fabricated using the most positive potential in the selected range, namely -300mV, to evaluate whether the lowest driving force was sufficient to ensure the progression of the electrodeposition. Despite the success of the procedure, the synthesized GDEs exhibited the highest electrical resistance and the lowest mass loading of all the samples analyzed (see Tab.4.1).

This is attributed to the low driving force applied during the process, which resulted in a slower mass transport rate, compared to the others. However, this mechanism ultimately led to uniform distribution of homogeneous Cu particles across the entire surface, with excellent surface coverage and roughness, as shown in Fig.4.3.

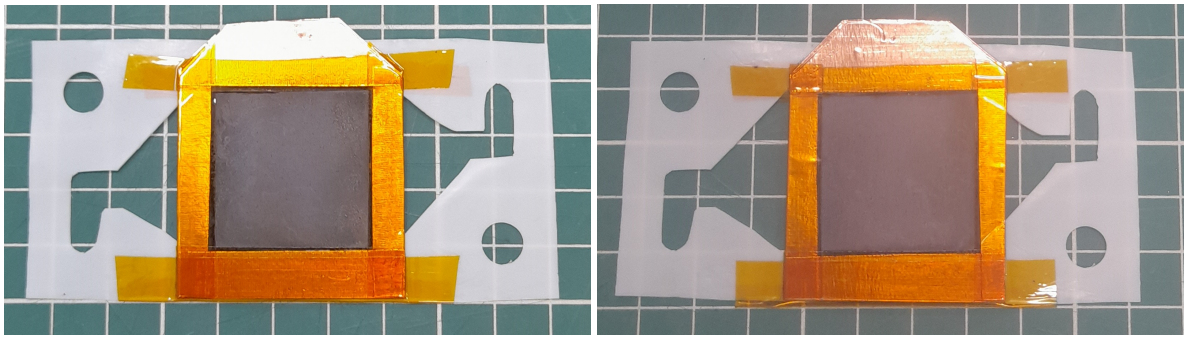

(a) Cu300 - n.1 (b) Cu300 - n.2

Figure 4.2: GDEs synthesized with potential fixed at -300mV.

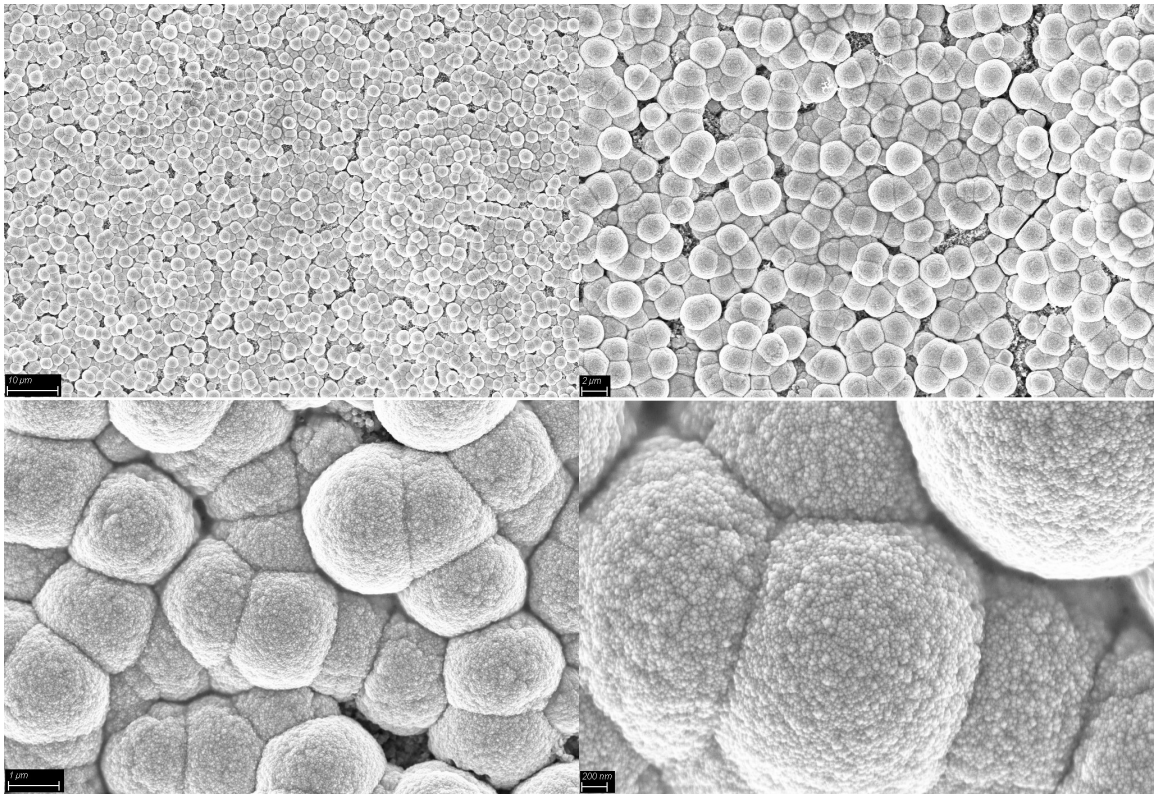

Figure 4.3: FESEM images of the Cu300 - n.1 at different magnification levels: 1K, 2.5K, 10K and 25K.

Table 4.1: Electrical resistance and mass loading: Cu300 comparison.

Sample	Resistance: before	Resistance: after	Mass Loading
N. 1	$\approx 400\ \Omega$	$80\ \Omega$	7.1 mg/cm^2
N. 2	$\approx 400\ \Omega$	$70\ \Omega$	8.1 mg/cm^2

4.1.2 Cu350 samples

The samples displayed in Fig.4.4 were fabricated using a less positive potential in the selected range, namely -350mV, to determine whether a small increase in the driving force may lead to some improvements. The procedure was successful and the synthesized GDEs revealed a decrease in electrical resistance accompanied by a slight increase in mass loading (see Tab.4.2). Nevertheless, the FESEM images did not show significant differences compared to the previous samples, as shown in Fig.4.5.

(a) Cu350 - n.1 (b) Cu350 - n.2

Figure 4.4: GDEs synthesized with potential fixed at -350mV.

Table 4.2: Electrical resistance and mass loading: Cu350 comparison.

Sample	Resistance: before	Resistance: after	Mass Loading
N. 1	$\approx 300\ \Omega$	$39\ \Omega$	9.4 mg/cm^2
N. 2	$\approx 400\ \Omega$	$36\ \Omega$	9.8 mg/cm^2

However, there was no evidence indicating whether such surface properties are more beneficial for the Ag displacement procedure and the CO_2RR, or if a less regular morphology would be preferable. Overall, the application of a moderate potential leads to a uniform and homogeneous distribution of the deposited material across the surface.

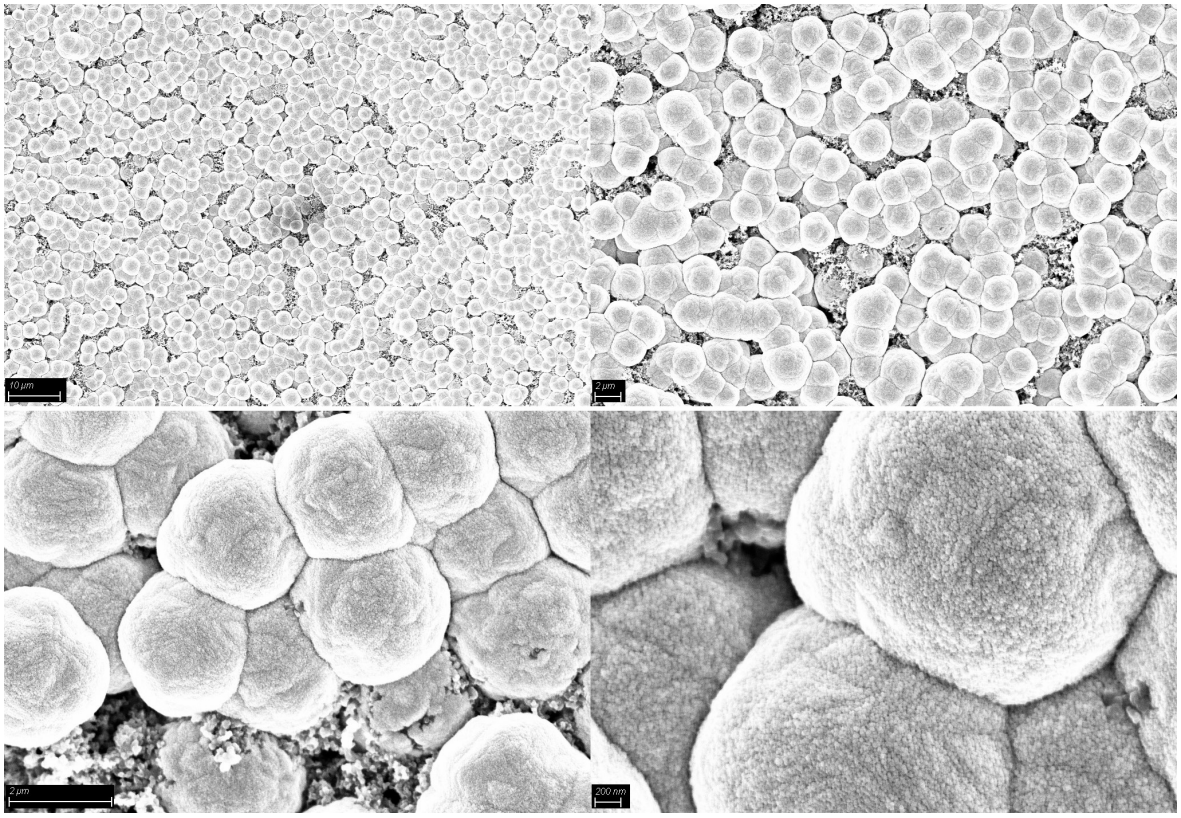

Figure 4.5: FESEM images of the Cu350 - n.1 at increasing magnification levels: 1K, 2.5K, 10K and 25K.

4.1.3 Cu400 samples

The samples displayed in Fig.4.6 were fabricated using the average potential in the selected range, namely -400mV, to understand how the dynamics of the phenomenon change when an even greater driving force is applied. After the completion of the process, the fabricated GDEs demonstrated a further increase in mass loading, but comparable electrical resistances (see Tab.4.3). Despite the similar surface properties with respect to the others samples, the formation of large Cu clusters is observed. This suggests that shifting the applied potential towards more negative values does not affect significantly mass transport, but rather influences the nucleation and agglomeration of particles, since their size increased rather than their number, as shown in Fig.4.7.

Table 4.3: Electrical resistance and mass loading: Cu400 comparison.

Sample	Resistance: before	Resistance: after	Mass Loading
N. 1	$\approx 200\ \Omega$	$37\ \Omega$	12.1 mg/cm^2
N. 2	$\approx 200\ \Omega$	$40\ \Omega$	10.4 mg/cm^2

(a) Cu400 - n.1 (b) Cu400 - n.2

Figure 4.6: GDEs synthesized with potential fixed at -400mV.

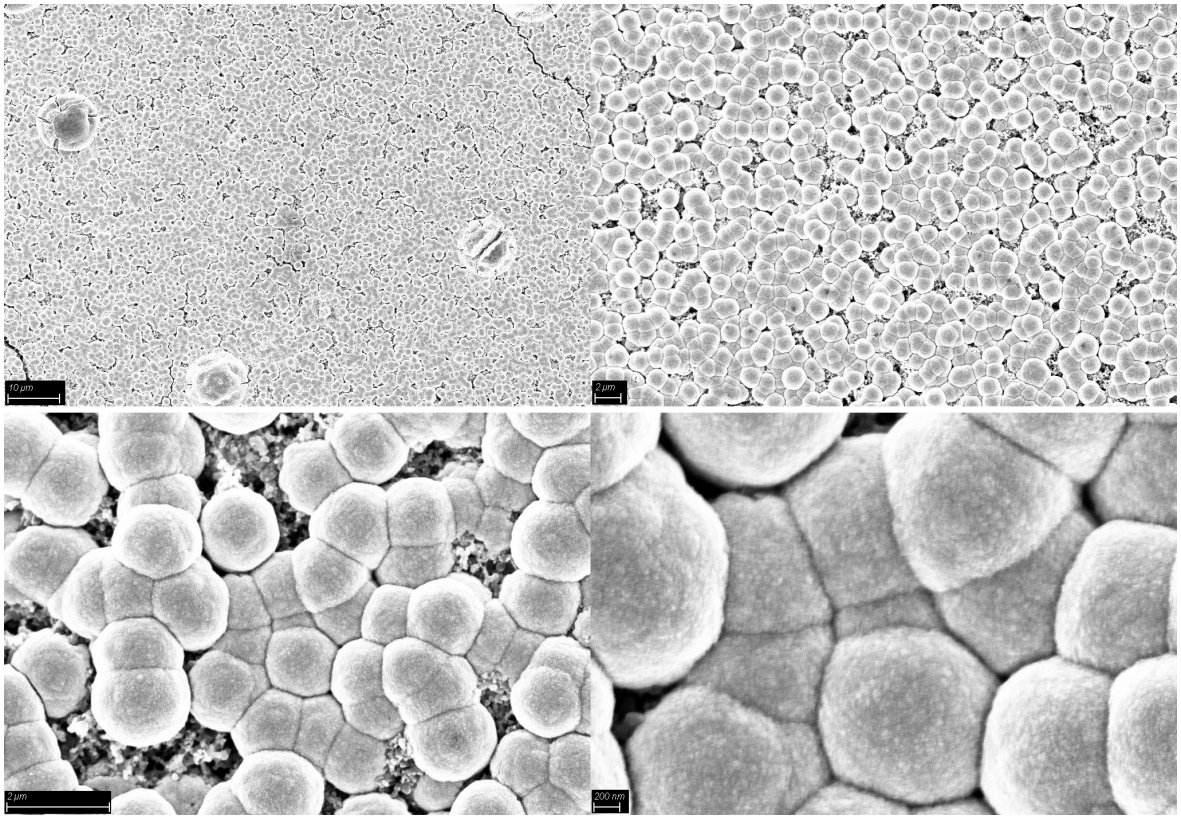

Figure 4.7: FESEM images of the Cu400 - n.1 at increasing magnification levels: 1K, 2.5K, 10K and 25K.

The samples shown so far are very similar to each other, thereby ensuring the reproducibility of the experiment for the chosen reaction conditions. However, only a selection of FESEM images is shown for the sake of simplicity.

4.1.4 Cu450 samples

The samples displayed in Fig.4.9 were fabricated using a even more potential in the selected range, namely -450mV, to assess the outcome of the deposition process when a strong driving force is employed. Upon completion of the procedure, the synthesized GDEs did not exhibit an increase in mass loading, neither a change in electrical resistances (see Tab.4.4). Nonetheless, FESEM images did show a variation in surface properties with respect to the previous samples, as the particle distribution changed significantly, resulting in samples with less mass coverage but, conversely, a larger active surface area, as shown in Fig.4.8.

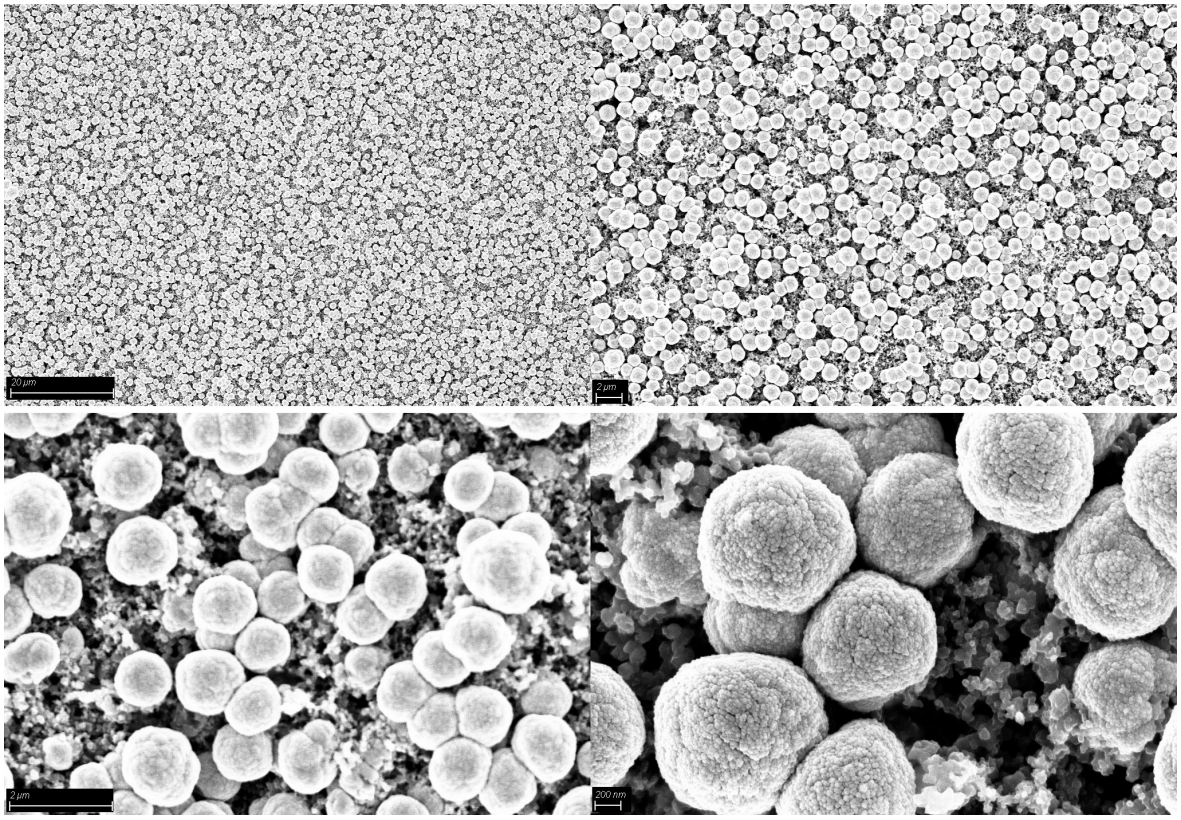

Figure 4.8: FESEM images of Cu450 - n.1 at increasing magnification levels: 1K, 2.5K, 10K and 25K.

Table 4.4: Electrical resistance and mass loading: Cu450 comparison.

Sample	Resistance: before	Resistance: after	Mass Loading
N. 1	$\approx 300\ \Omega$	$38\ \Omega$	10.7 mg/cm^2
N. 2	$\approx 400\ \Omega$	$39\ \Omega$	10.1 mg/cm^2

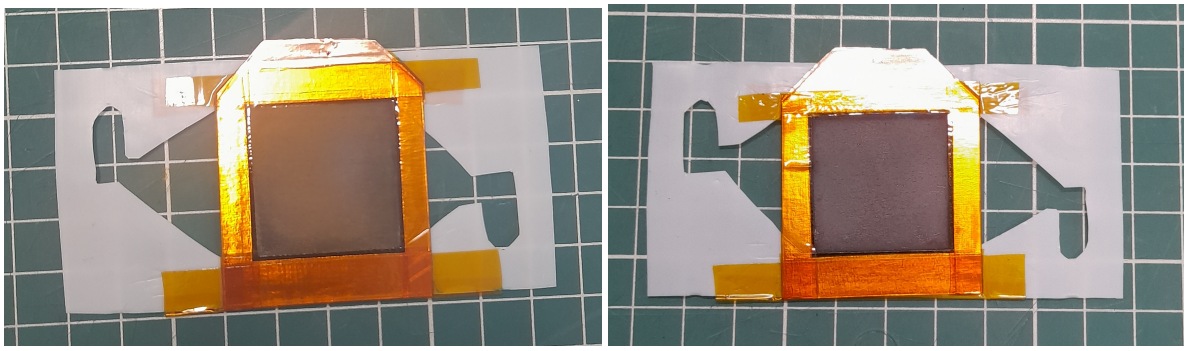

(a) Cu450 - n.1 (b) Cu450 - n.2

Figure 4.9: GDEs synthesized with potential fixed at -450mV.

4.1.5 Cu500 samples

The samples displayed in Fig.4.10 were fabricated using the most negative potential in the selected range, namely -500mV, to evaluate whether applying a really high driving force contributed to advancements in the understanding of the electrodeposition process. As a result of the procedure, the fabricated GDEs showed the highest mass loading among all the samples analyzed, while maintaining comparable electrical resistances (see Tab.4.5). This can be attributed to the fact that applying a highly negative potential enhances reaction kinetics during electrodeposition, as it provides a stronger driving force for the electrochemical processes. It accelerates the reduction and deposition of Cu ions onto the substrate, thus promoting particle agglomeration and resulting in increased surface roughness. The presence of massive Cu clusters is evident, resulting in a highly irregular surface morphology, as shown in Fig.4.11.

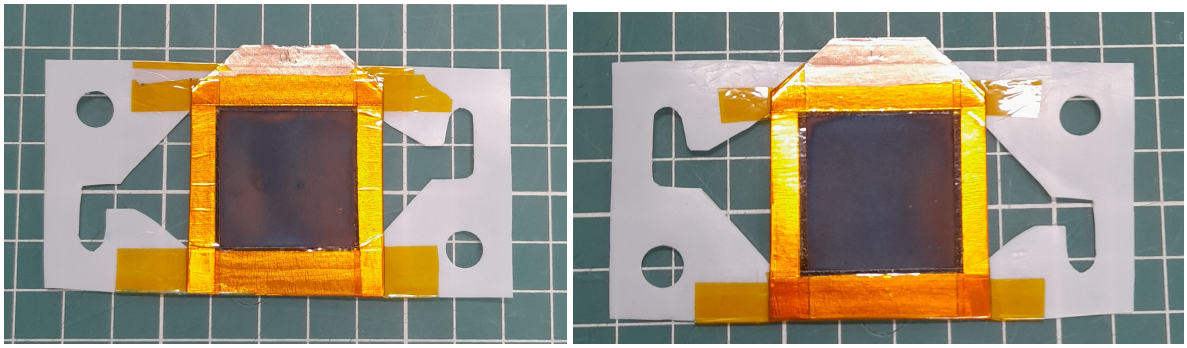

(a) Cu500 - n.1 (b) Cu500 - n.2

Figure 4.10: GDEs synthesized with potential fixed at -500mV.

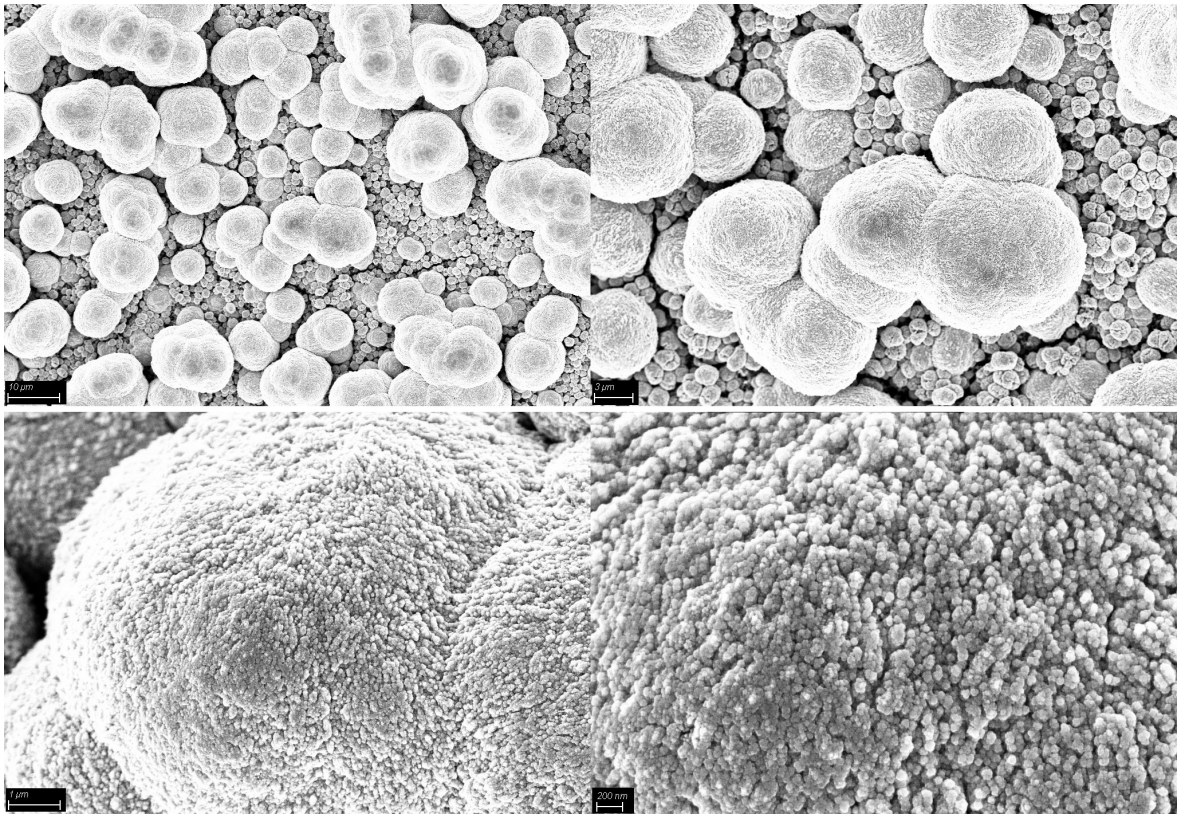

Figure 4.11: FESEM images of Cu500 - n.1 at increasing magnification levels: 1K, 2.5K, 10K and 25K.

Table 4.5: Electrical resistance and mass loading: Cu500 comparison.

Sample	Resistance: before	Resistance: after	Mass Loading
N. 1	$\approx 600\ \Omega$	$30\ \Omega$	17.5 mg/cm^2
N. 2	$\approx 300\ \Omega$	$40\ \Omega$	13.4 mg/cm^2

4.1.6 Cu-Ag samples

While the synthesis of Cu-based GDEs was primarily aimed at understanding and optimizing the electrodeposition process, some of the fabricated samples were subjected to Ag displacement in an attempt to exploit the tandem effect to steer the reaction product selectivity. In addition, such procedure is very simple and enables a meaningful comparison of the Cu-Ag GDEs with the monometallic ones, both to evaluate their electrochemical performance and to assess the success of the Ag replacement. The samples displayed in Fig.4.12 and Fig.4.14 were fabricated from Cu350 and Cu400 electrodes, as they provided both a uniform and homogeneous surface morphology, which in turn resulted in bimetallic surfaces sharing similar physical properties.

The replacement mechanism occurred uniformly across the entire surface enhancing both the surface roughness and the extent of the active surface area. Nevertheless, distinct morphological changes were observed, such as the appearance of brighter, compact regions characterized by needle-shaped or crystal-like formations, as shown in Fig.4.13 and Fig.4.15 respectively, corresponding to Ag-rich domains.

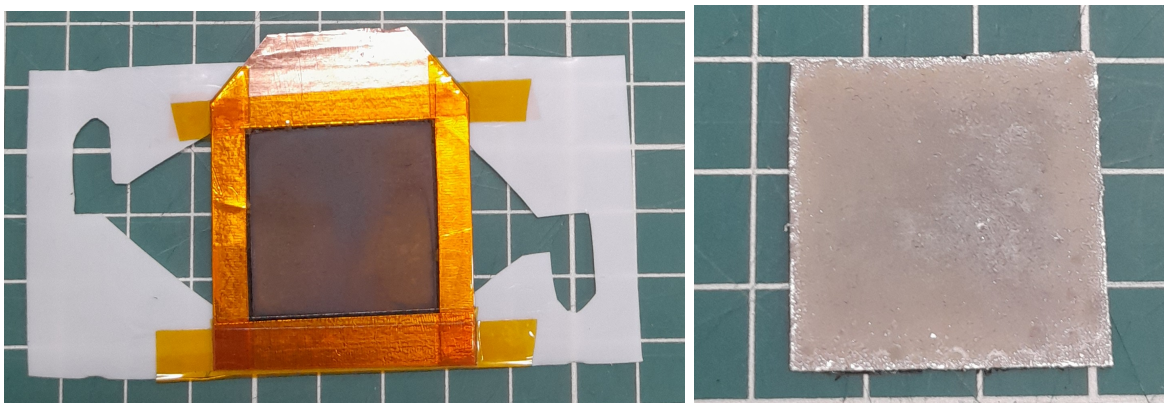

(a) Cu350 (b) Cu350-Ag

Figure 4.12: Bimetallic GDE synthesized with potential fixed at -350mV.

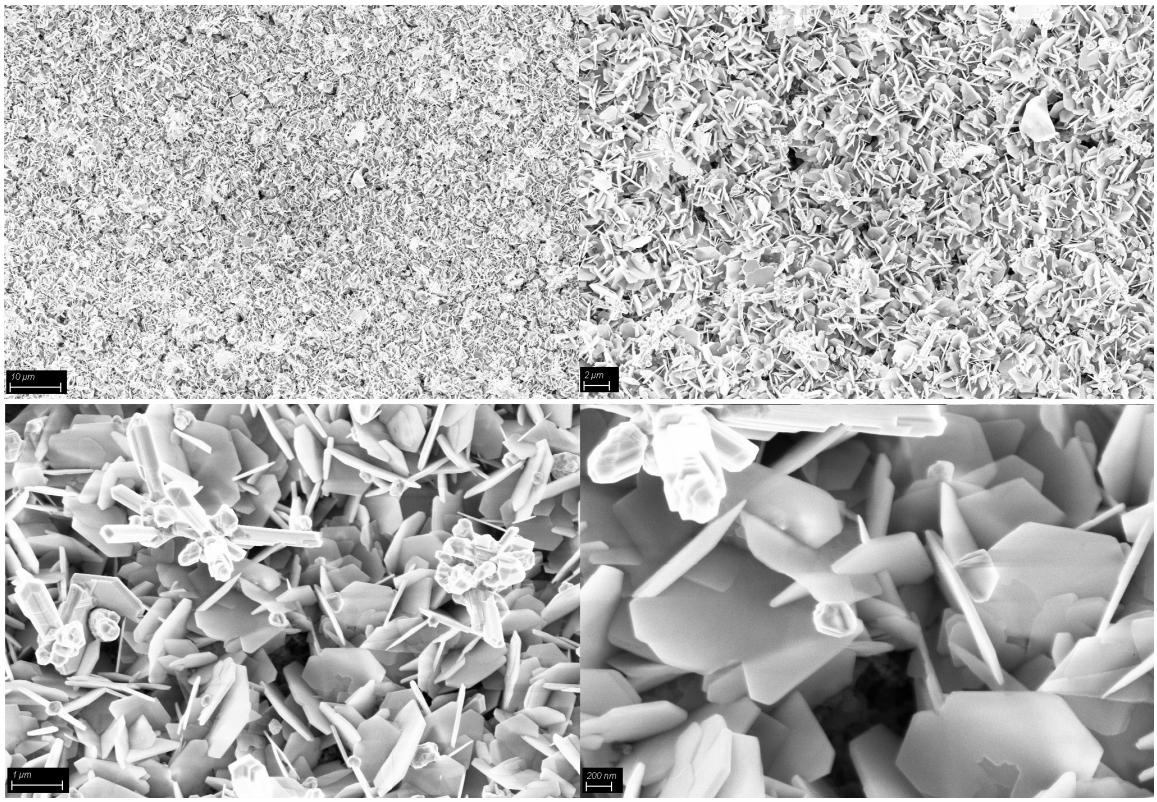

Figure 4.13: Cu350-Ag images at increasing magnification levels: 1K, 2.5K, 10K, 25K.

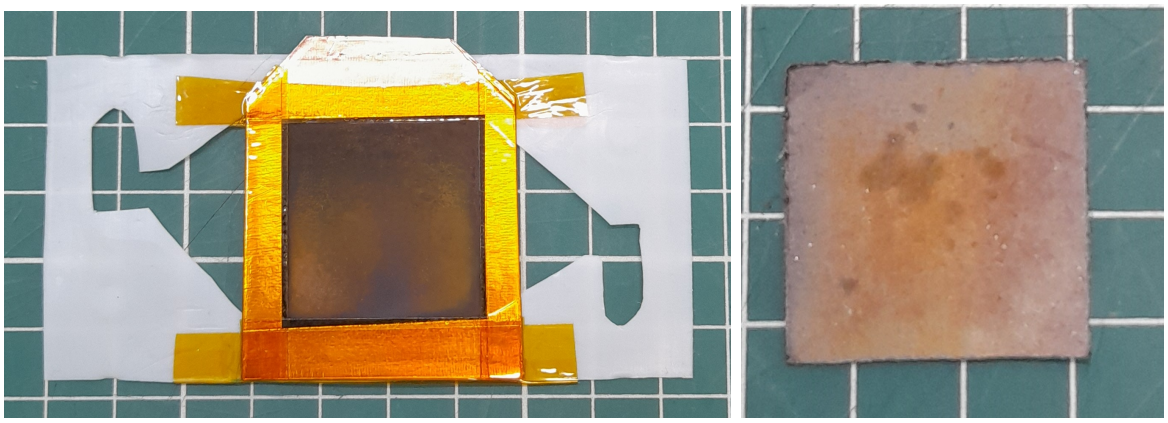

(a) Cu400 (b) Cu400-Ag

Figure 4.14: Bimetallic GDE synthesize with potential fixed at -400mV.

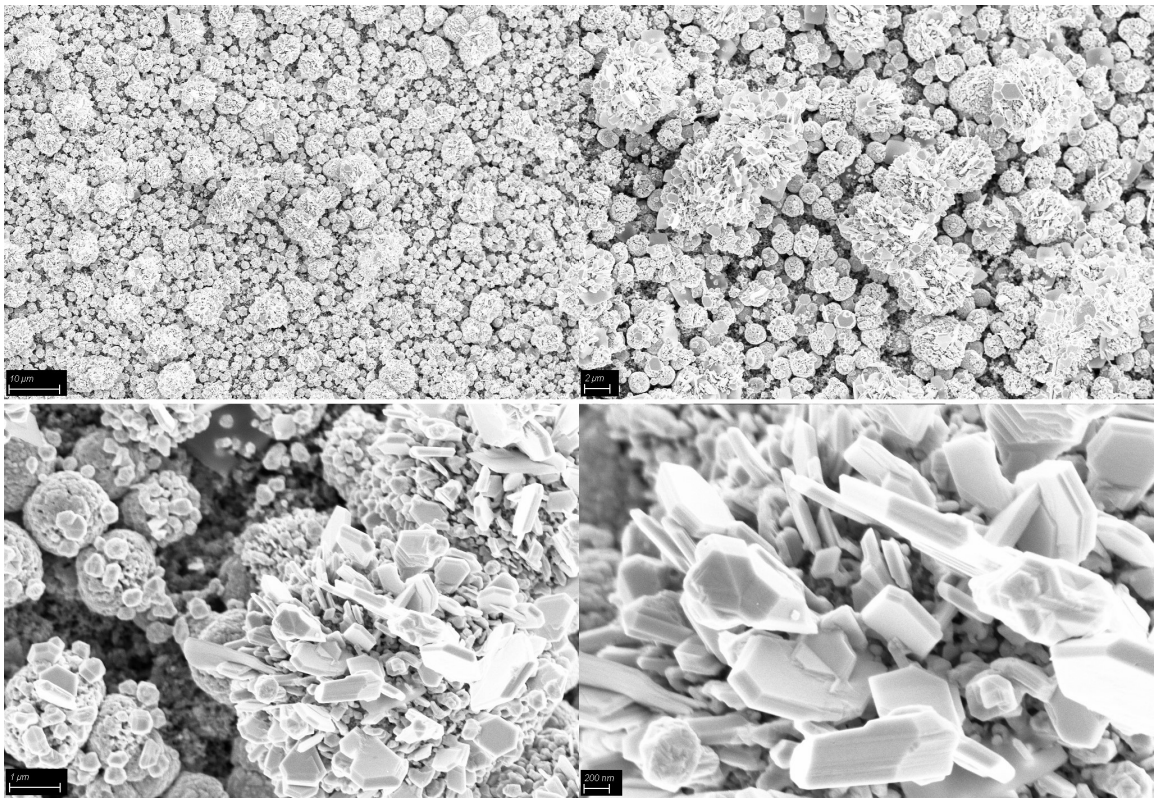

Figure 4.15: Cu400-Ag images at increasing magnification levels: 1K, 2.5K, 10K, 25K.

To conclude the physical characterization, it can be observed that deposition at low negative potentials results in a uniform and homogeneous Cu surface distribution. Meanwhile, as the magnitude of the potential increases, the morphology becomes progressively more irregular, and large Cu clusters begin to form.

Additionally, the mass loading appears to be directly proportional to the driving force intensity, whereas the electrical resistance does not seem to be affected by the magnitude of the applied potential. In general, the mass coverage determines the uniformity of the Cu distribution and thus the reproducibility of the experiments, while the number active sites influence the reaction kinetics, as they control how much CO_2 can be reduced simultaneously. Hence, balancing these two properties by appropriately tuning the deposition potential is crucial to maximize the conversion efficiency. Finally, EDS analysis demonstrated the presence of Ag following the displacement process (see Fig.4.16), specifically with a Cu:Ag molar ratio of 1.92 and 2.57 for the Cu350-Ag and Cu400-Ag respectively. However, the successful fabrication of GDEs alone does not guarantee the effectiveness of the materials toward the CO_2RR, which must be assessed through experimental testing in MEA cells.

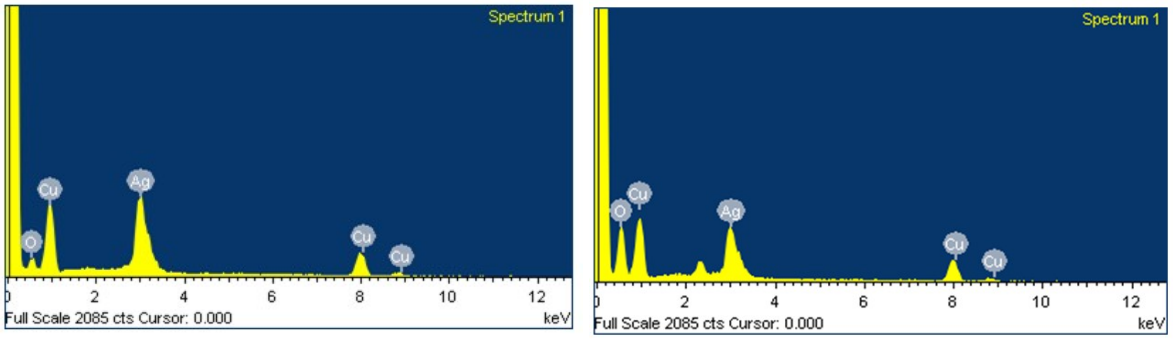

(a) EDS analysis on Cu350-Ag

(b) EDS analysis on Cu400-Ag

Figure 4.16: Compositional analysis of the bimetallic GDEs.

4.2 Electrochemical characterization

The electrochemical characterization provides essential insight into the catalytic activity, selectivity and stability of the prepared samples. The following sections present the results for Cu-based and Cu-Ag bimetallic GDEs, highlighting the differences or similarities in onset potential, short-term stability and charge-transfer behavior:

1. LSV was performed to evaluate the onset potential of the catalysts for the CO_2RR. During LSV tests, the samples exhibited a noticeable increase in current density at high potentials, indicating the activation of CO_2 reduction pathways. Moreover, reduction peaks were observed at low potentials, clearly indicating the reduction of the outermost Cu oxide particles during the measurement.

2. PEIS measurements were conducted to investigate charge-transfer kinetics related to each GDEs, while also confirming the correct setup of the cell through consistent resistance values, evaluated through the study of the Nyquist plots. This step was essential prior to the subsequent tests to ensure proper functioning of the system and verify the absence of short circuits.

3. CP experiments, performed at constant current density, were used to probe the selectivity and short-term stability of the GDEs under continuous operation. The tested samples showed stable overall performance, although minor potential fluctuations were observed, suggesting partial deactivation likely caused by surface restructuring occurring during the process. In general, the CP tests provided an estimation of the FE by correlating the sustained current with the quantity of detected products.

4.2.1 Monometallic catalysts

Typically, the CO_2RR inside the MEA cell setup occurs at potentials exceeding the value of 3 V, as shown by the noticeable increase in current density response of the Cu-based GDEs tested with LSV (see Fig.4.17, 4.18). Moreover, reduction peaks are observed at potentials between 2 - 3 V, suggesting that the outhermost Cu oxide layer, developed during exposure of the samples to air, is reduced due to the applied potential. Overall, most of the fabricated GDEs tested in MEA cell demonstrated a maximum achievable current significantly higher than that required for the subsequent CP testing, which is 1000 mA, thereby guaranteeing the CO_2 electrolysis at 200 mA/cm^2 at a reasonable cell voltage. This outcome is crucial to future industrial applications.

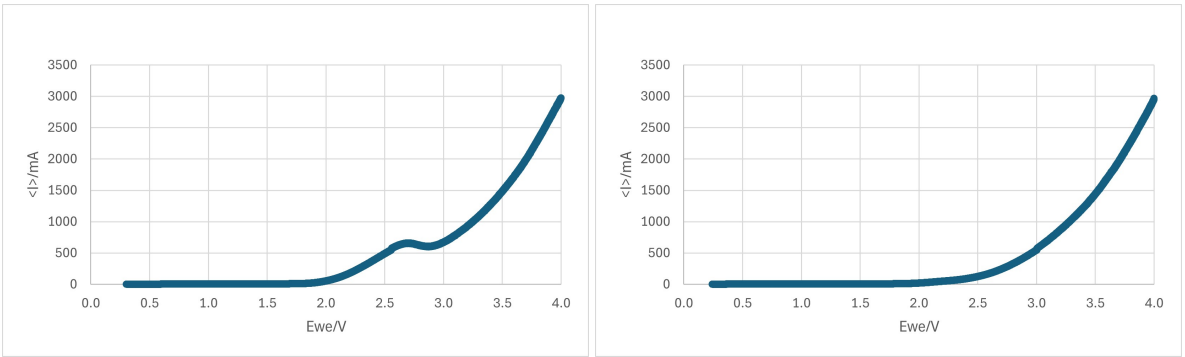

(a) First LSV attempt on Cu350 - n.1 (b) Second LSV attempt on Cu350 - n.1

Figure 4.17: LSV study on Cu350 sample, shown in Fig.4.4a.

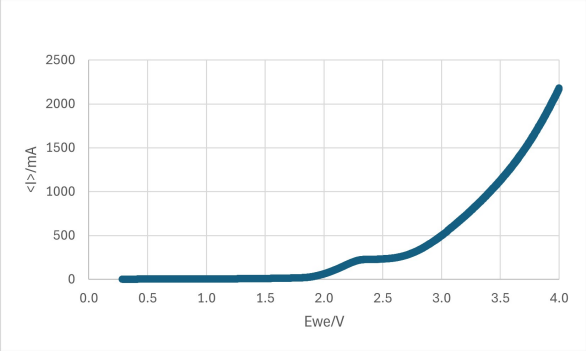

(a) First LSV attempt on Cu450 - n.1

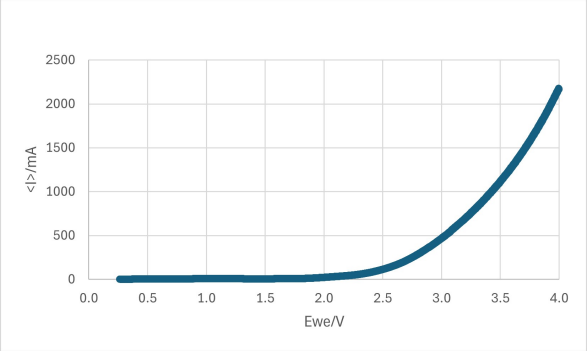

(b) Second LSV attempt on Cu450 - n.1

Figure 4.18: LSV study on Cu450 sample, shown in Fig.4.9a.

The electrical resistance measurements were conducted to verify the proper functioning of the AEM employed, which would otherwise hinders charge-transfer kinetics, and the correct assembly of the cell. Since this parameter is only partially influenced by the GDEs conformation and is instead primarily determined by the operating environment, which is kept constant, we expect the measured values to be very similar across the tested samples, as shown in Fig.4.19.

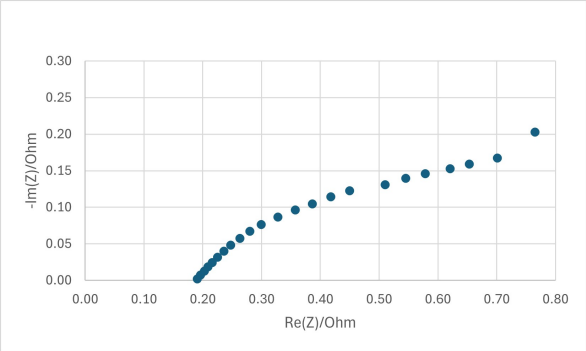

(a) PEIS on Cu350 - n.1, see Fig4.4a

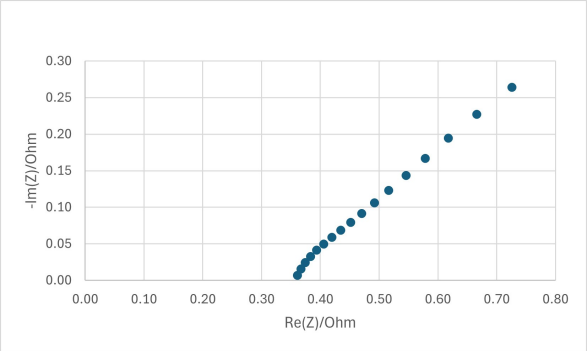

(b) PEIS on Cu450 - n.1, see Fig.4.9a.

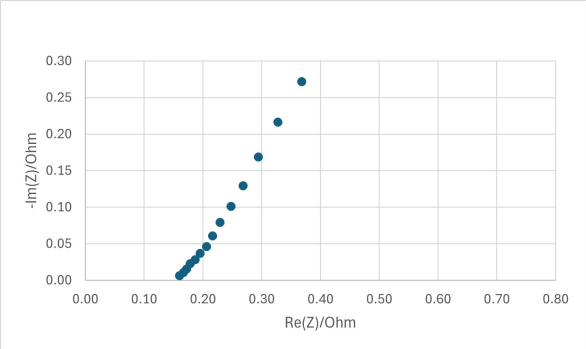

(c) PEIS on Cu300 - n.2, see Fig4.2b

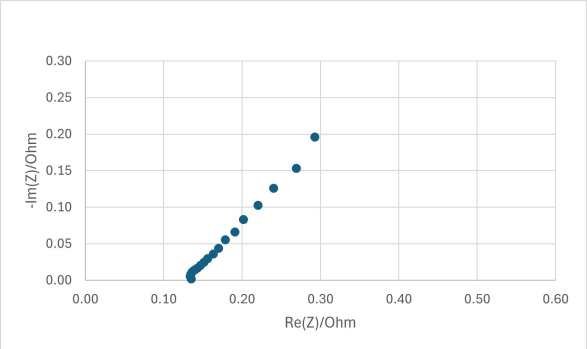

(d) PEIS on Cu500 - n.2, see Fig.4.10b.

Figure 4.19: Electrical resistance measurements on Cu GDEs

In general, within the MEA experimental setup, values in the range of 0.1 Ω to 0.3 Ω are considered indicative of normal operation. Values above this threshold, instead, typically signal a malfunction or a deviation from expected behavior. The samples under analysis did not exhibit any significant issues and can therefore be subjected to subsequent CP experiments.

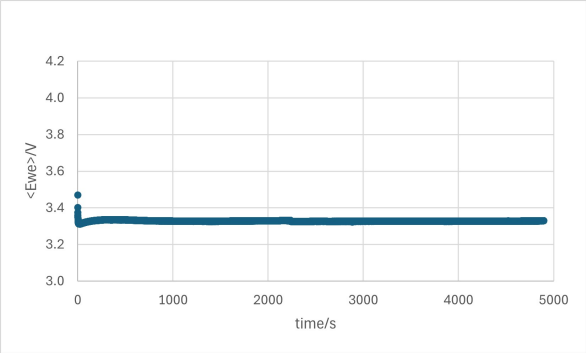

(a) CP on Cu350 - n.1, see Fig4.4a

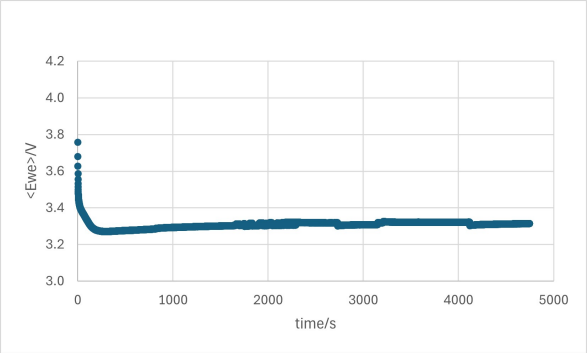

(b) CP on Cu450 - n.1, see Fig.4.9a.

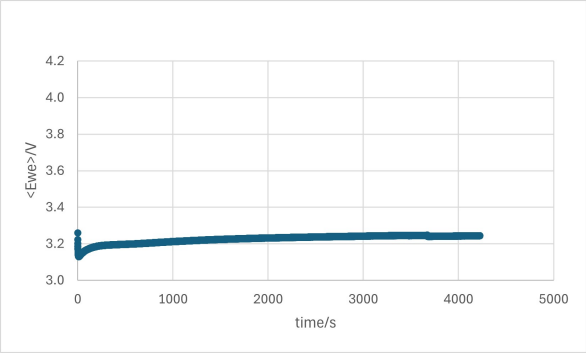

(c) CP on Cu300 - n.2, see Fig4.2b

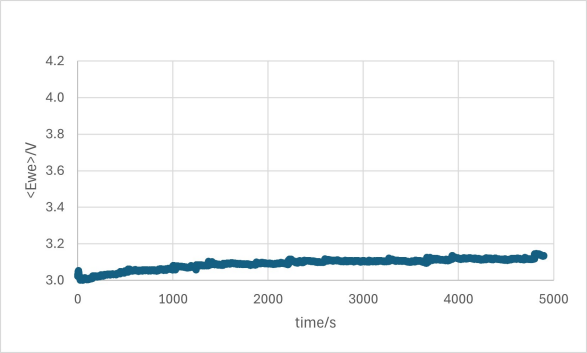

(d) CP on Cu500 - n.2, see Fig.4.10b.

Figure 4.20: Voltage response to fixed current density of -200 mA/cm^2.

CP measurements are central to the overall electrochemical characterization, as they closely reproduce the real operating conditions of the GDEs. Under steady-state galvanostatic conditions, once the MEA cell voltage exceeds the activation threshold for the CO_2RR, the catalysts are expected to initiate the electrochemical conversion of CO_2, thereby fulfilling their intended function. In general, a stable potential is desirable, as it reflects uniform reaction conditions. Conversely, potential fluctuations are indicative of an unstable working environment, which can negatively affect the ongoing electrochemical process. All analyzed samples showed stable performance for the CO_2RR under the tested conditions (see Fig.4.20), although long-term stability assessments remain necessary. Notably, the Cu500 GDE exhibit local potential fluctuations, which are likely attributable to their distinct morphology.

4.2.2 Bimetallic catalysts

The Cu-Ag bimetallic catalysts exhibited performance closely comparable to their monometallic counterparts, with respect to both maximum current density and activation potential (see Fig.4.21). The reduction peaks were also observed, likely attributable mainly to Cu rather than Ag, as the latter one is a nobler metal and therefore less susceptible to oxidation. However, the possibility that Ag was also reduced during the measurement cannot be excluded.

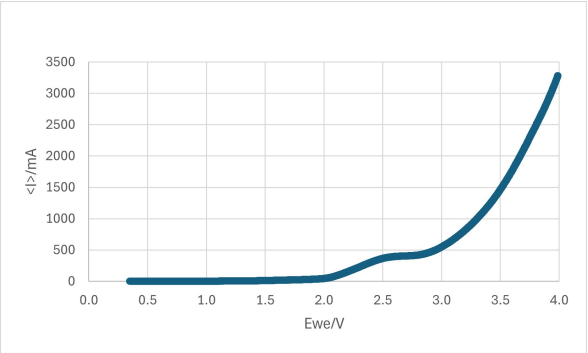

(a) LSV on Cu400-Ag, see Fig.4.14b

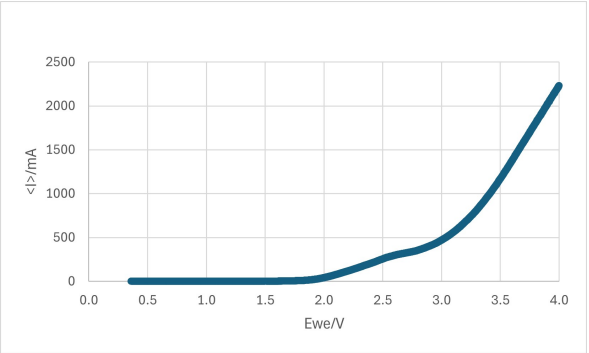

(b) LSV on Cu350-Ag, see Fig.4.12b

Figure 4.21: LSV study on Cu350-Ag and Cu400-Ag samples

The measured resistance values are consistent with those of previously studied samples and ensure the proper functioning of the cell, as shown in Fig.4.22.

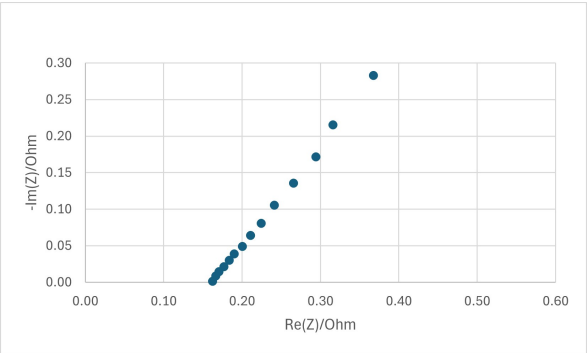

(a) PEIS on Cu400-Ag, see Fig4.14b

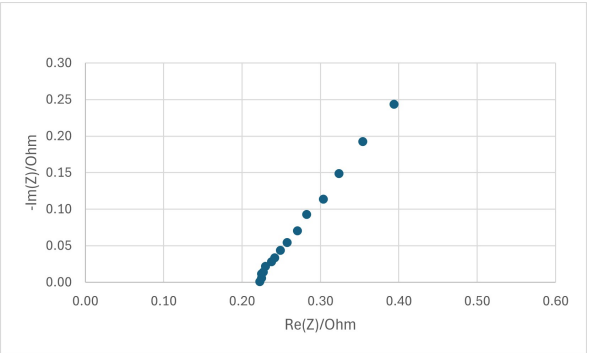

(b) PEIS on Cu350-Ag, see Fig.4.12b.

Figure 4.22: Electrical resistance measurements on Cu350-Ag and Cu400-Ag GDEs

Similar considerations apply to the CP tests (see Fig.4.23), which exhibit good short-term stability and appropriate voltages for the CO_2RR. The presence of Ag does not appear to significantly affect the dynamics of the experiment, although a slight increase in voltage response at the same applied current is observed compared to the monometallic GDEs.

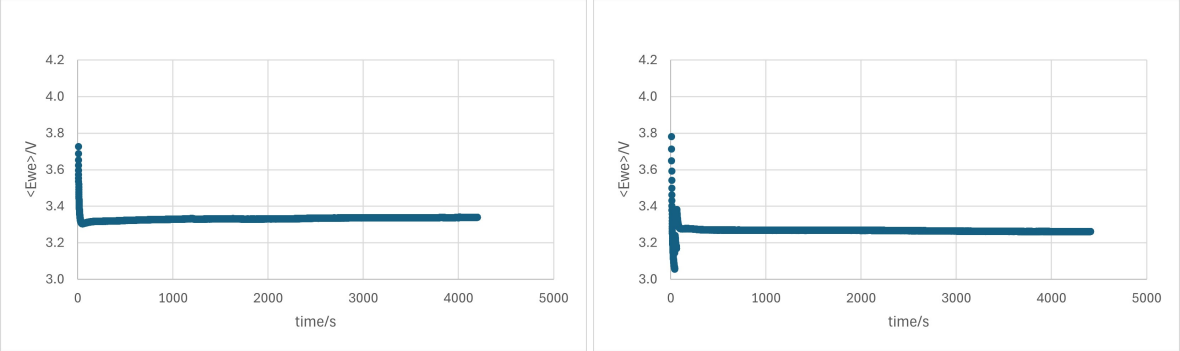

(a) CP on Cu400-Ag, see Fig4.14b

(b) CP on Cu350-Ag, see Fig.4.12b.

Figure 4.23: Voltage response to fixed current density of -200 mA/cm^2.

4.3 Products analysis

Electrochemical activity alone does not provide a complete picture of the catalysts performance. Product analysis is essential to determine selectivity, efficiency, and the practical relevance of the prepared GDEs. The following sections present the results obtained from gas and liquid phase analysis of the Cu-based and Cu-Ag samples.

4.3.1 Gas selectivity

The selectivity toward the following gas products was assessed using through Eq.3.1:

1. H_2: Hydrogen is typically the most significant competing product, originating from the HER. Its formation reduces the overall selectivity toward carbon-based products, as a large fraction of the current is consumed by this side process.

2. CO: Carbon monoxide is a two-electron product commonly generated on metals and is a key intermediate for multi-carbon products. When it desorbs rapidly, CO is obtained as the final product, where if it remains adsorbed it can undergo further reductions.

3. C_2H_4: Ethylene is one of the most valuable C_{2+} products. It is primarily used as a precursor for the production of polyethylene, the most widely employed plastic worldwide, as well as others polymers such as polyvinyl chloride (PVC). Moreover, it is also essential for the synthesis of industrial chemicals and polyester fibers, which are commonly used in the textile and apparel industry due to their durability and cost-effectiveness.

4. C_2H_6: Ethane is a valuable feedstock in the petrochemical sector. It is used as a fuel and as a potential energy carrier, due to its relatively clean combustion compared to heavier hydrocarbons.

Overall, the Cu-based GDEs exhibit a steady production of H_2 and CO, as these are typical products of the CO_2RR. The competing HER hinders the formation of multi-carbon products by occupying most of the catalytic active sites with *H intermediates and thereby preventing the proper adsorption and further reductions of *CO intermediates, which therefore obstacles C_{2+} product formation. This issue can worsen over the course of the measurement due to system malfunctions, such as membrane failure or restructuring of the Cu. Nevertheless, a significant amount of C_2H_4 was produced, with FE values exceeding 20%, while C_2H_6 was detected only in trace quantities, as shown in Fig.4.24. Although identifying the best-performing sample is not straightforward, the poorest performance was observed for the Cu500 sample, which was fabricated at the most negative applied voltage. It appears that an irregular morphology is unable to provide a stable working environment, and therefore negatively affects performance, particularly in terms of stability, as an overly reactive surface tends to degrade and restructure quickly.

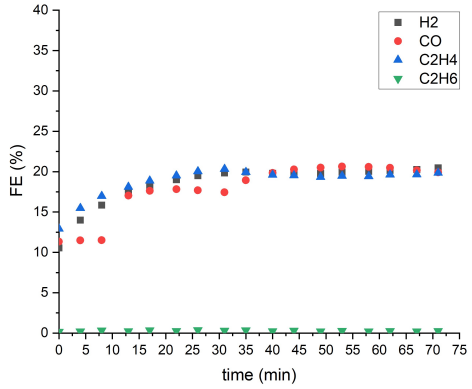

(a) Gas FEs of Cu350 - n.1, see Fig4.4a

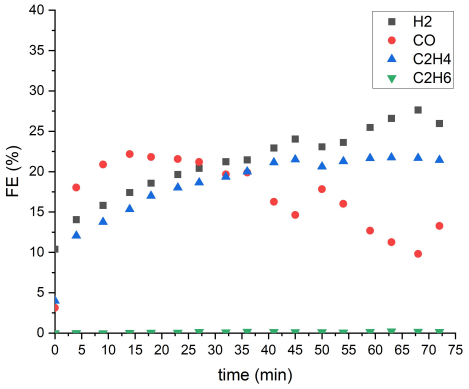

(b) Gas FEs of Cu450 - n.1, see Fig.4.9a.

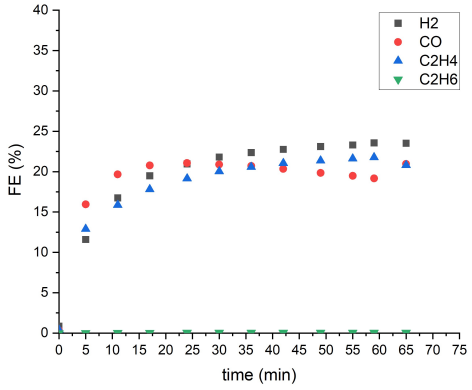

(c) Gas FEs of Cu300 - n.2, see Fig4.2b

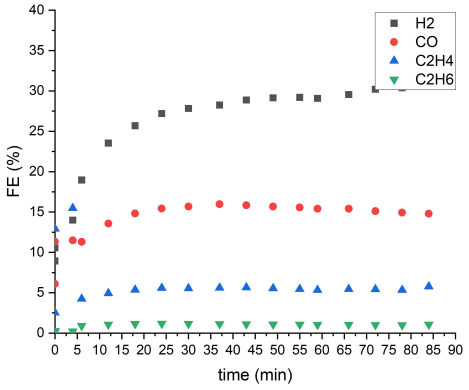

(d) Gas FEs of Cu500 - n.2, see Fig.4.10b.

Figure 4.24: Gaseous product selectivity over time.

A similar trend is observed for the bimetallic GDEs (see Fig.4.25), which show no substantial variation in selectivity, regardless of the incorporation of a second metallic element. On the contrary, a decline in performance is observed, marked by an increased production of H_2, which, according to the literature that guided the design of these catalysts, should have been suppressed. This effect is probably related to the wettability of the electrode surface. Although no catholyte is used in the MEA configuration, the cathode surface is in contact with the membrane, which exhibits a high water uptake capability. The addition of Ag to the surface may have increased the hydrophilicity of the Cu electrode, thereby enhancing its wettability and thereby resulting in higher HER rates. Futher experiments, such as contact angle measurements, are required to proof this hypothesis.

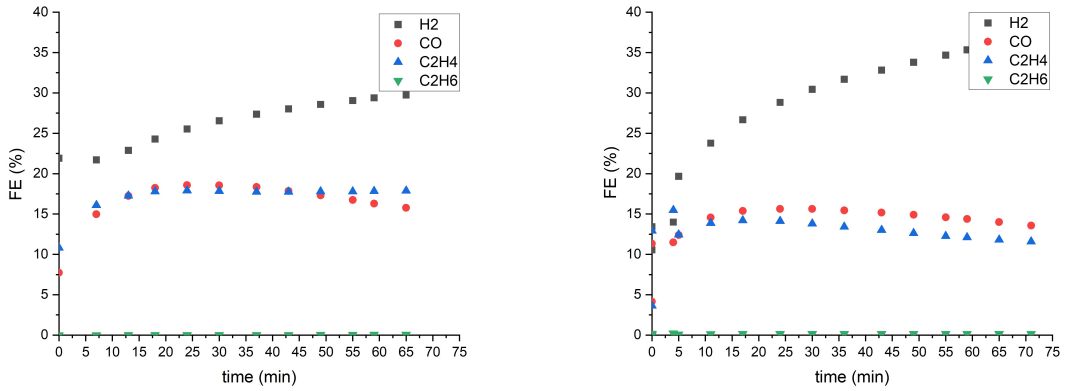

(a) Gas FEs of Cu400-Ag, Fig4.14b

(b) Gas FEs of Cu350-Ag, Fig.4.12b.

Figure 4.25: Gaseous product selectivity over time during the CP4.23.

In general, all samples appear to be only marginally influenced by surface morphology or material composition, as they exhibit similar selectivity trends. Perhaps, a more uniform surface coverage correlates with greater reliability and stability of the results. In conclusion, while the electrodeposition method enables straightforward synthesis of GDEs for the CO_2RR in MEA configuration, it provides limited control over the selectivity toward gaseous products. Furthermore, the incorporation of Ag through displacement did not yield the expected improvements, as demonstrated in this study.

4.3.2 Liquid selectivity

The liquid selectivity toward the following products was determined using Eq.3.2:

1. HCOOH: Formic acid is a simple carboxylic acid obtained through two-electron reduction of CO_2. It is common reaction intermediate and it is employed in chemical manufacturing as a preservative or reducing agent for the synthesis of more complex chemicals.

2. CH_3COOH: Acetic acid is small organic acid, used in industry as a platform chemical, meaning that it serves as a starting point to make other important compounds. For example, it is essential to produce vinyl acetate and cellulose acetate, which are building blocks of adhesives, plastics and fibers.

3. CH_3CH_2OH: Ethanol is a simple alcohol with high energy density, widely used as solvent for chemicals and pharmaceuticals. It can be employed as bio-fuel or fuel additive, since it can be burned directly or blended with gasoline, thus helping reducing reliance on fossil fuels.

Overall, both the Cu-based and the Cu-Ag GDEs demonstrated good selectivity toward HCOOH, as expected given that it is an easily accessible single-carbon product, and CH_3CH_2OH, with FEs approaching a value of 10%. Meanwhile, CH_3COOH was detected only in trace amounts. The following graphs (see Fig.4.26,4.27) present the sum of the selectivities calculated for the analyzed GDEs, allowing a visual and concise appreciation of their performance in terms of CO_2 conversion.

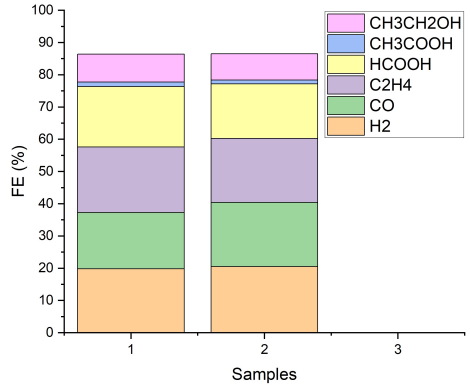

(a) Total FEs of Cu350 - n.1, see Fig4.4a

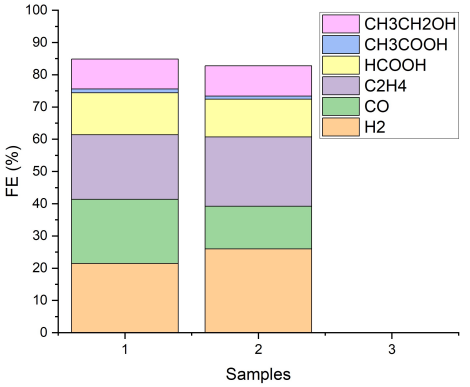

(b) Total FEs of Cu450 - n.1, see Fig.4.9a.

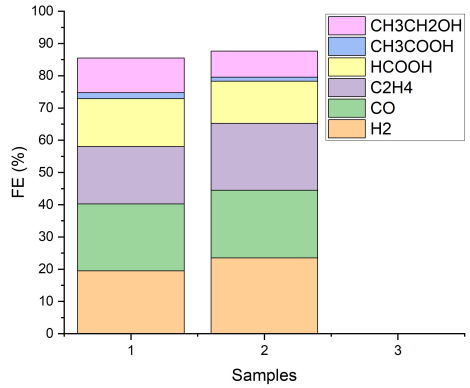

(c) Total FEs of Cu300 - n.2, see Fig4.2b

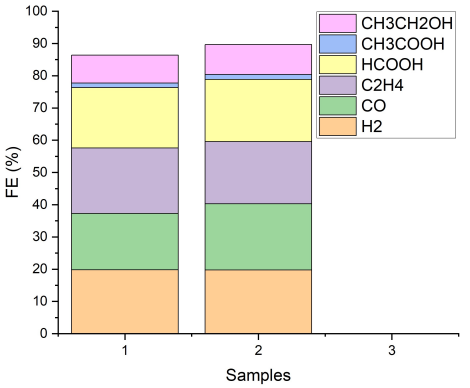

(d) Total FEs of Cu500 - n.2, see Fig.4.10b.

Figure 4.26: Complete product selectivity of the Cu GDEs.

Samples 1 and 2 represent the liquid samples collected at the midpoint and at the end of the measurement, respectively, appropriately integrated with the corresponding gas samplings. In general, the total selectivity did not reach 100%, likely due to product losses during operation as well as limitations in the analytical procedure, which, for the sake of computational simplicity, may have resulted in an small underestimation of products. Also in this instance, the presence of a second metallic element did not result in any appreciable change in the reaction pathways.

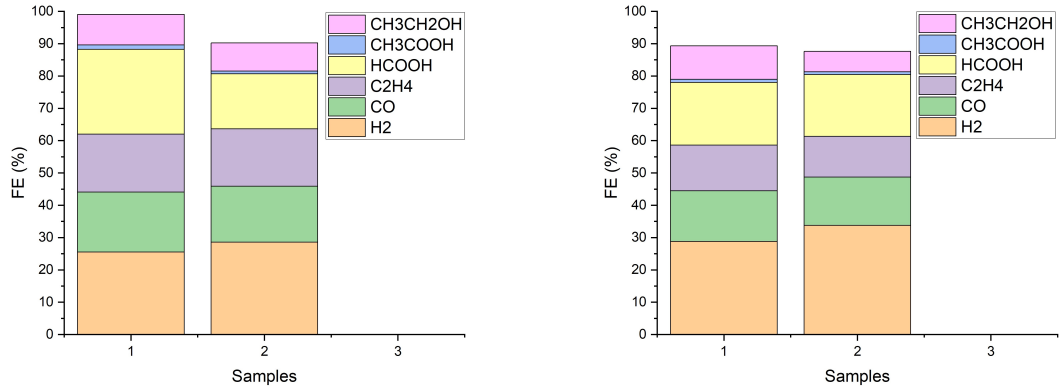

(a) Total FEs of Cu400-Ag, see Fig4.14b (b) Total FEs of Cu350-Ag, see Fig.4.12b.

Figure 4.27: Complete product selectivity of Cu-Ag GDEs

Although the selectivity toward valuable reaction products was successfully achieved, a significant challenge persists in directing it toward a narrower and more defined range of products. Achieving such specificity is crucial, as it would greatly facilitate the subsequent separation and collection processes, ultimately enhancing the overall efficiency and practicality of the catalytic system. Moreover, despite promising indications, uncertainties still remain regarding the effective utilization of the catalytic capabilities of Ag. Further investigation is required to fully understand the role that this noble metal plays when coupled with Cu for the CO_2RR and to optimize its incorporation for improved bimetallic systems.

CHAPTER 5

Conclusion and future perspectives

This thesis work has shown that Cu electrodeposition on GDL carbon paper represents a valid alternative to more sophisticated techniques such as sputtering or chemical vapor deposition for the fabrication of GDEs aimed at CO_2 conversion in a MEA cell configuration. Unlike these methods, electrodeposition offers the advantages of being simpler, more cost-effective and easily scalable. Moreover, the process is inherently flexible, as tuning the deposition parameters such as potential and time allows modulation of the morphology of the resulting metallic electrodes.

The electrochemical characterization and subsequent product analysis demonstrated the successful outcome of the CO_2RR. In particular, the detection of ethylene and ethanol highlights the ability of the synthesized GDEs to generate products with significant industrial and energetic value. Nevertheless, the variations in catalysts surface morphology did not translate into noticeable changes in reaction product selectivity. Similarly, the introduction of Ag through a displacement reaction, despite being successfully carried out on Cu-based samples, did not lead to a significant shift in the FEs. These findings suggest that, although the electrodeposition strategy provides a versatile and simple pathway to produce functional GDEs, the underlying mechanisms that govern the selectivity remain insufficiently understood.

Future studies should therefore aim at unraveling the complex relationships between the GDEs surface morphology and resulting reaction pathways during the CO_2RR. Further deposition experiments are required, particularly under conditions distinct from those previously examined. For instance, the co-deposition of Cu and Ag may result in more uniform bimetallic structures or even the formation of alloys. Additionally, the Cu to Ag ratio could be more precisely controlled using such an approach. Therefore, the electrodeposition process presented here provides a foundation for the fabrication of Cu–Ag and other Cu-based bimetallic electrodes.

A more comprehensive and diverse physical characterization can also facilitate the optimization of the fabrication process. Moreover, electrochemical tests should be conducted over a wide range of current densities to enable a comprehensive comparison of all samples. In addition, employing electrolytes with compositions and properties different from those previously used could provide a better understanding of the samples performance under varying operating conditions.

Ultimately, all these efforts have been driven by a collective ambition: to transform one of the greatest challenges of our time, the rising concentration of CO_2, into an opportunity for innovation and hope. By advancing the understanding of catalyst material preparation for electrochemical conversion of such greenhouse gas, this work aims to take a small yet meaningful step toward a future in which science and technology play a pivotal role in mitigating climate change and building a more sustainable world.

Acknowledgements

Voglio dedicare un amorevole riconoscimento alla mia famiglia, ai miei genitori e a mio fratello. Voi siete i pilastri che mi hanno sorretto durante questo percorso, donandomi sia la possibilità di intraprenderlo che la forza di portarlo a termine. Con voi condivido la gioia e la leggerezza che questo traguardo mi regala, forte della consapevolezza di essere ora un uomo risoluto. La vostra perpetua presenza nel mio cuore è come una splendida fiamma che arde e che illumina coloro che mi son cari con le stesso sentimento che mi avete sempre offerto: la speranza.

Un prezioso e affettuoso ringraziamento rivolgo inoltre ai miei fantastici amici e ai miei amati cugini. Avete contribuito a rendere la mia esperienza di vita unica e degna di essere vissuta. Le corde della mia anima suonano dolcemente in vostra compagnia e suonano una melodia così speciale da non poterla descrivere a parole. Conservo come un tesoro il ricordo di tutte le giornate passate assieme e sorrido di gratitudine alle avventure che ancora ci aspettano.

Ringrazio con profondo rispetto i miei relatori, chè mi hanno guidato e istruito lungo questo percorso di continue scoperte. La premura con cui ho ricevuto le conoscenze necessarie al mio lavoro mi ha permesso di studiare con passione e interesse. Sono stato fortunato ad avervi ricevuto come miei maestri.

Infine, rendiamo omaggio a questi indimenticabili versi:

Considerate la vostra semenza:
fatti non foste a viver come bruti,
ma per seguir virtute e canoscenza.

Bibliography

[1] Rattan Lal. Soil carbon sequestration impacts on global climate change and food security. *Science*, 304(5677):1623–1627, 2004.

[2] Susan Solomon, Gian-Kasper Plattner, Reto Knutti, and Pierre Friedlingstein. Irreversible climate change due to carbon dioxide emissions. *Proceedings of the National Academy of Sciences*, 106(6):1704–1709, 2009.

[3] S. Chu, Y. Cui, and N. Liu. The path towards sustainable energy. *Nature Materials*, 16:16–22, 2016.

[4] Genxiang Wang, Junxiang Chen, Yichun Ding, Pingwei Cai, Luocai Yi, Yan Li, Chaoyang Tu, Yang Hou, Zhenhai Wen, and Liming Dai. Electrocatalysis for co_2 conversion: from fundamentals to value-added products. *Chemical Society Reviews*, 50(8):4993–5061, 2021.

[5] D. Kim, K. K. Sakimoto, D. Hong, and P. Yang. Artificial photosynthesis for sustainable fuel and chemical production. *Angewandte Chemie International Edition*, 54:3259–3266, 2015.

[6] Douglas R. Kauffman, Jay Thakkar, Rajan Siva, Christopher Matranga, Paul R. Ohodnicki, Chenjie Zeng, and Rongchao Jin. Efficient electrochemical co_2 conversion powered by renewable energy. *ACS Applied Materials & Interfaces*, 7(28): 15626–15632, 2015.

[7] Jan Mertens, Ronnie Belmans, and Michael E. Webber. Why the carbon-neutral energy transition will imply the use of lots of carbon. *C—Journal of Carbon Research*, 6(2), 2020.

[8] M. Jouny, W. Luc, and F. Jiao. General techno-economic analysis of co_2 electrolysis systems. *Industrial Engineering Chemistry Research*, 57(6):2165–2177, 2018.

[9] Oleksandr S. Bushuyev, Phil De Luna, Cao-Thang Dinh, Ling Tao, Garth Saur, Joost de Lagemaat, Sheryl O. Kelley, and Edward H. Sargent. What should we make with co_2 and how can we make it? *Joule*, 2(5):825–832, 2018.

[10] A. S. Agarwal, Y. Zhai, D. Hill, and N. Sridhar. The electrochemical reduction of carbon dioxide to formate/formic acid: Engineering and economic feasibility. *ChemSusChem*, 4:1301–1310, 2011.

[11] Jan Mertens, Christian Breyer, Katrin Arning, André Bardow, Ronnie Belmans, Angela Dibenedetto, Suren Erkman, Jim Gripekoven, Grégoire Léonard, Sylvain Nizou, Deepak Pant, Ana S. Reis-Machado, Peter Styring, Jaap Vente, Michael Webber, and Célia J. Sapart. Carbon capture and utilization: More than hiding co_2 for some time. *Joule*, 7(3):442–449, 2023.

[12] Shuyu Liang, Naveed Altaf, Liang Huang, Yanshan Gao, and Wang Qiang. Electrolytic cell design for electrochemical co_2 reduction. *Journal of CO2 Utilization*, 35:90–105, jan 2020.

[13] Erdogan Alper and Ozge Yuksel Orhan. Co_2 utilization: Developments in conversion processes. *Petroleum*, 3(1):109–126, 2017.

[14] Hyung-Kyu Lim and Hyungjun Kim. The mechanism of room-temperature ionic-liquid-based electrochemical co_2 reduction: A review. *Molecules*, 22(4):536, 2017.

[15] Sichao Ma and A. Kenis, Paul J.˙ Electrochemical conversion of co_2 to useful chemicals: current status, remaining challenges, and future opportunities. *Current Opinion in Chemical Engineering*, 2(2):191–199, 2013.

[16] Da-Ming Feng, Yun-Pei Zhu, Ping Chen, and Tian-Yi Ma. Recent advances in transition-metal-mediated electrocatalytic co_2 reduction: From homogeneous to heterogeneous systems. *Catalysts*, 7(12):373, 2017.

[17] C. Graves, S. D. Ebbesen, M. Mogensen, and K. S. Lackner. Sustainable hydrocarbon fuels by recycling CO_2 and H_2O with renewable or nuclear energy. *Renewable and Sustainable Energy Reviews*, 15:1–23, 2011.

[18] A. Goeppert, M. Czaun, J.-P. Jones, G. K. Surya Prakash, and G. A. Olah. Recycling of carbon dioxide to methanol and derived products – closing the loop. *Chemical Society Reviews*, 43:7995–8048, 2014.

[19] Ke Li, Bo Peng, and Tianyou Peng. Recent advances in heterogeneous photocatalytic co_2 conversion to solar fuels. *ACS Catalysis*, 6(11):7485–7527, 2016.

[20] S. Verma, B. Kim, Hsuan-Te Rickey Jhong, S. Ma, and P. J. A. Kenis. A gross-margin model for defining technoeconomic benchmarks in the electroreduction of co_2. *ChemSusChem*, 9(15):1972–1979, 2016.

[21] R. Kortlever, J. Shen, K. J. P. Schouten, F. Calle-Vallejo, and M. T. M. Koper. Catalysts and reaction pathways for the electrochemical reduction of carbon dioxide. *The Journal of Physical Chemistry Letters*, 6(20):4073–4082, 2015.

[22] Kendra P. Kuhl, Etosha R. Cave, David N. Abram, and Thomas F. Jaramillo. New insights into the electrochemical reduction of carbon dioxide on metallic copper surfaces. *Energy & Environmental Science*, 5(5):7050–7059, 2012.

[23] Lei Fan, Chuan Xia, Fangqi Yang, Jun Wang, Haotian Wang, and Yingying Lu. Strategies in catalysts and electrolyzer design for electrochemical co_2 reduction toward c_{2+} products. *Science Advances*, 6(8):eaay3111, 2020.

[24] Xiaolong Zhang, Si-Xuan Guo, Karl A. Gandionco, Alan M. Bond, and Jie Zhang. Electrocatalytic carbon dioxide reduction: from fundamental principles to catalyst design. *Materials Today Advances*, 7:100074, 2020.

[25] Yuhou Pei, Heng Zhong, and Fangming Jin. A brief review of electrocatalytic reduction of co_2 — materials, reaction conditions, and devices. *Energy Science & Engineering*, 9(7):1012–1032, 2021.

[26] Sahil Garg, Mengran Li, Adam Z. Weber, Lei Ge, Liye Li, Victor Rudolph, Guoxiong Wang, and Thomas E. Rufford. Advances and challenges in electrochemical co_2 reduction processes: an engineering and design perspective looking beyond new catalyst materials. *Journal of Materials Chemistry A*, 8(4):1511–1544, 2020.

[27] Allen J. Bard and Larry R. Faulkner. *Electrochemical Methods: Fundamentals and Applications*. Wiley, New York, 2 edition, 2001.

[28] Joseph Wang. *Analytical Electrochemistry*. John Wiley & Sons, Hoboken, NJ, 3rd edition, 2006.

[29] Allen J. Bard. Inner-sphere heterogeneous electrode reactions. electrocatalysis and photocatalysis: The challenge. *Journal of the American Chemical Society*, 132(22):7559–7567, 2010.

[30] Marco Dunwell, Yushan Yan, and Bingjun Xu. Understanding the influence of the electrochemical double-layer on heterogeneous electrochemical reactions. *Current Opinion in Chemical Engineering*, 20:151–158, 2018.

[31] Louisa Rui Lin Ting, Oriol Piqué, SiYing Lim, Mohammad Tanhaei, Federico Calle-Vallejo, and BoonSiang Yeo. Enhancing co_2 electroreduction to ethanol on copper–silver composites by opening an alternative catalytic pathway. *ACS Catalysis*, 10(7):4059–4069, 2020.

[32] Heng Zhong, Katsushi Fujii, and Yoshiaki Nakano. Effect of $khco_3$ concentration on electrochemical reduction of co_2 on copper electrode. *Journal of The Electrochemical Society*, 164(9):F923–F927, 2017.

[33] Hiroshi Hashiba, Lien-Chun Weng, Yikai Chen, Hiroki K. Sato, Satoshi Yotsuhashi, Chengxiang Xiang, and Adam Z. Weber. Effects of electrolyte buffer capacity on surface reactant species and the reaction rate of co_2 in electrochemical co_2 reduction. *The Journal of Physical Chemistry C*, 122(7):3719–3726, 2018.

[34] Neeraj Gupta, Michael Gattrell, and Barry MacDougall. Calculation for the cathode surface concentrations in the electrochemical reduction of co_2 in $khco_3$ solutions. *Journal of Applied Electrochemistry*, 36(2):161–172, 2006.

[35] Fen Zhang and Anne C. Co. Direct evidence of local ph change and the role of alkali cation during co_2 electroreduction in aqueous media. *Angewandte Chemie International Edition*, 59(4):1674–1681, 2020.

[36] C. S. Chen, A. D. Handoko, J. H. Wan, L. Ma, D. Ren, and B. S. Yeo. Stable and selective electrochemical reduction of carbon dioxide to ethylene on copper mesocrystals. *Catalysis Science & Technology*, 5:161–168, 2015.

[37] Devin T. Whipple and Paul J. A. Kenis. Prospects of co_2 utilization via direct heterogeneous electrochemical reduction. *Journal of Physical Chemistry Letters*, 1(24):3451–3458, 2010.

[38] Tu N. Nguyen and Cao-Thang Dinh. Gas diffusion electrode design for electrochemical carbon dioxide reduction. *Chemical Society Reviews*, 49(21):7488–7504, 2020.

[39] X. Nie, M. R. Esopi, M. J. Janik, and A. Asthagiri. Selectivity of co_2 reduction on copper electrodes: The role of the kinetics of elementary steps. *Angewandte Chemie International Edition*, 52:2459–2462, 2013.

[40] Xiaowa Nie, Monica R. Esopi, Michael J. Janik, and Aravind Asthagiri. Selectivity of co_2 reduction on copper electrodes: The role of the kinetics of elementary steps. *Angewandte Chemie International Edition*, 52(9):2459–2462, 2013.

[41] Dan Ren, Yilin Deng, Albertus D. Handoko, Chung Shou Chen, Souradip Malkhandi, and Boon Siang Yeo. Selective electrochemical reduction of carbon dioxide to ethylene and ethanol on copper(i) oxide catalysts. *ACS Catalysis*, 5(5): 2814–2821, 2015.

[42] K. P. Kuhl, E. R. Cave, D. N. Abram, and T. F. Jaramillo. New insights into the electrochemical reduction of carbon dioxide on metallic copper surfaces. *Energy Environmental Science*, 5:7050–7059, 2012.

[43] M. Gattrell, N. Gupta, and A. Co. A review of the aqueous electrochemical reduction of co_2 to hydrocarbons at copper. *Journal of Electroanalytical Chemistry*, 594:1–19, 2006.

[44] Y. Hori, H. Wakebe, T. Tsukamoto, and O. Koga. Electrocatalytic process of co selectivity in electrochemical reduction of co_2 at metal electrodes in aqueous media. *Electrochimica Acta*, 39:1833–1839, 1994.

[45] Yoshio Hori, Osamu Koga, Hiroki Yamazaki, and Tadanori Matsuo. Infrared spectroscopy of adsorbed co and intermediate species in electrochemical reduction of co_2 to hydrocarbons on a cu electrode. *Electrochimica Acta*, 40(16):2617–2622, 1995.

[46] Yoshio Hori, Akira Murata, and Ryutaro Takahashi. Formation of hydrocarbons in the electrochemical reduction of carbon dioxide at a copper electrode in aqueous solution. *Journal of the Chemical Society, Faraday Transactions 1: Physical Chemistry in Condensed Phases*, 85(8):2309–2326, 1989.

[47] A. A. Peterson, F. Abild-Pedersen, F. Studt, J. Rossmeisl, and J. K. Nørskov. How copper catalyzes the electroreduction of carbon dioxide into hydrocarbon fuels. *Energy & Environmental Science*, 3:1311–1315, 2010.

[48] F. Calle-Vallejo and M. T. M. Koper. Theoretical considerations on the electroreduction of co to c_2 species on cu(100) electrodes. *Angewandte Chemie International Edition*, 52:7282–7285, 2013.

[49] Andrew A. Peterson, Frank Abild-Pedersen, Felix Studt, Jan Rossmeisl, and Jens K. Nørskov. How copper catalyzes the electroreduction of carbon dioxide into hydrocarbon fuels. *Energy & Environmental Science*, 3(9):1311–1315, 2010.

[50] Hailing Wang, Xiangji Zhou, Tianshui Yu, Xianglong Lu, Lihua Qian, Pan Liu, and Pengxiang Lei. Surface restructuring in agcu single-atom alloy catalyst and self-enhanced selectivity toward co_2 reduction. *Electrochimica Acta*, 426:140774, 2022.

[51] Tianrui Lu, Ting Xu, Shaojun Zhu, Jun Li, Jichang Wang, Huile Jin, Xin Wang, Jing-Jing Lv, Zheng-Jun Wang, and Shun Wang. Electrocatalytic co_2 reduction to ethylene: From advanced catalyst design to industrial applications. *Advanced Materials*, 35(52):e2310433, 2023.

[52] Rulle Reske, Hemma Mistry, Farzad Behafarid, Beatriz Roldan Cuenya, and Peter Strasser. Particle size effects in the catalytic electroreduction of co_2 on cu nanoparticles. *Journal of the American Chemical Society*, 136(19):6978–6986, 2014.

[53] Ming Ma, Bartek J. Trześniewski, Jie Xie, and Wilson A. Smith. Selective and efficient reduction of carbon dioxide to carbon monoxide on oxide-derived nanostructured silver electrocatalysts. *Angewandte Chemie International Edition*, 55 (33):9748–9752, 2016.

[54] Xiong Peng, Stavros G. Karakalos, and William E. Mustain. Preferentially oriented ag nanocrystals with extremely high activity and faradaic efficiency for co_2 electrochemical reduction to co. *ACS Applied Materials Interfaces*, 10(2):1734–1742, 2018.

[55] Yoshio Hori, Hidetoshi Wakebe, Toshio Tsukamoto, and Osamu Koga. Electrocatalytic process of co selectivity in electrochemical reduction of co_2 at metal electrodes in aqueous media. *Electrochimica Acta*, 39(11–12):1833–1839, 1994.

[56] Drew C. Higgins, Alan Taylor Landers, Yongfei Ji, Stephanie Anne Nitopi, Carlos Gilberto Morales Guio, Lei Wang, Karen Chan, Christopher Hahn, and Thomas Jaramillo. Guiding electrochemical carbon dioxide reduction toward carbonyls using copper silver thin films with interphase miscibility. *ACS Energy Letters*, 3(12):2947–2955, nov 2018.

[57] T. Hatsukade, K. P. Kuhl, E. R. Cave, D. N. Abram, and T. F. Jaramillo. Insights into the electrocatalytic reduction of co_2 on metallic silver surfaces. *Physical Chemistry Chemical Physics*, 16(28):13814–13819, 2014.

[58] E. L. Clark, C. Hahn, T. F. Jaramillo, and A. T. Bell. Electrochemical co_2 reduction over compressively strained cuag surface alloys with enhanced multi-carbon oxygenate selectivity. *Journal of the American Chemical Society*, 139(44):15848–15857, 2017.

[59] T. T. H. Hoang, S. Verma, S. Ma, T. T. Fister, J. Timoshenko, A. I. Frenkel, P. J. A. Kenis, and A. A. Gewirth. Nanoporous copper–silver alloys by additive-controlled electrodeposition for the selective electroreduction of co_2 to ethylene and ethanol. *Journal of the American Chemical Society*, 140(17):5791–5797, 2018.

[60] Cheng Du, Joel P. Mills, Asfaw G. Yohannes, Wei Wei, Lei Wang, Siyan Lu, Jian-Xiang Lian, Maoyu Wang, Tao Guo, Xiyang Wang, Hua Zhou, Cheng-Jun Sun, John Z. Wen, Brian Kendall, Martin Couillard, Hongsheng Guo, ZhongChao Tan, Samira Siahrostami, and Yimin A. Wu. Cascade electrocatalysis via agcu single-atom alloy and ag nanoparticles in co_2 electroreduction toward multicarbon products. *Nature Communications*, 14:6142, 2023.

[61] Juqin Zeng, Michele Re Fiorentin, Marco Fontana, Micaela Castellino, Francesca Risplendi, Adriano Sacco, Giancarlo Cicero, Mohammadamin Farkhondehfal, Filippo Drago, and Candido F. Pirri. Novel insights into sb-cu catalyst for elec-

trochemical reduction of co_2. *Applied Catalysis B: Environmental*, 306:121089, 2022.

[62] P. C. K. Vesborg and B. Seger. Performance limits of photoelectrochemical co_2 reduction based on known electrocatalysts and the case for two-electron reduction products. *Chemistry of Materials*, 28:8844–8850, 2016.

[63] Aijun Vasileff, Chen Xu, Yang Jiao, Yang Zheng, and Shi-Zhang Qiao. Surface and interface engineering in copper-based bimetallic materials for selective co_2 electroreduction. *Chem*, 4(8):1809–1831, 2018.

[64] Tianyu Zheng, Kai Jiang, and Haotian Wang. Recent advances in electrochemical co_2-to-co conversion on heterogeneous catalysts. *Advanced Materials*, 30(18): 1802066, 2018.

[65] Zhen Chang, Shuang Huo, Wenhua Zhang, Jinghuai Fang, and Hui Wang. The tunable and highly selective reduction products on ag@cu bimetallic catalysts toward co_2 electrochemical reduction reaction. *The Journal of Physical Chemistry C*, 121(21):11368–11379, 2017.

[66] Thuy Tien H. Hoang, Santosh Verma, Siyuan Ma, Timothy T. Fister, Janis Timoshenko, Anatoly I. Frenkel, Paul J. A. Kenis, and Andrew A. Gewirth. Nanoporous copper–silver alloys by additive-controlled electrodeposition for the selective electroreduction of co_2 to ethylene and ethanol. *Journal of the American Chemical Society*, 140(17):5791–5797, 2018.

[67] Dohyung Kim, Chenlu Xie, Nigel Becknell, Yi Yu, Mohammadreza Karamad, Karen Chan, Ethan J. Crumlin, Jens K. Nørskov, and Peidong Yang. Electrochemical activation of co_2 through atomic ordering transformations of aucu nanoparticles. *Journal of the American Chemical Society*, 139(24):8329–8336, 2017.

[68] Ji Hoon Lee, Shyam Kattel, Zhao Jiang, Zhenhua Xie, Siyu Yao, Brian M. Tackett, Wenqian Xu, Nebojsa S. Marinkovic, and Jingguang G. Chen. Tuning the activity and selectivity of electroreduction of co_2 to synthesis gas using bimetallic catalysts. *Nature Communications*, 10:3724, 2019.

[69] Yanwei Lum and Joel W. Ager. Sequential catalysis controls selectivity in electrochemical co_2 reduction on cu. *Energy & Environmental Science*, 11:2935–2944, 2018.

[70] Gurudayal, Daniele Perone, Shubham Malani, Yan Lum, Sophia Haussener, and Joel W. Ager. Sequential cascade electrocatalytic conversion of carbon dioxide to c–c coupled products. *ACS Applied Energy Materials*, 2(6):4551–4559, 2019.

[71] Antonia Herzog, Arno Bergmann, Hyo Sang Jeon, Janis Timoshenko, Stefanie Kühl, Clara Rettenmaier, Mauricio Lopez Luna, Felix T. Haase, and Beatriz Roldan Cuenya. Operando investigation of ag-decorated cu_2o nanocube catalyst with enhanced co_2 electroreduction toward liquid products. *Angewandte Chemie International Edition*, 60(13):7426–7435, 2021.

[72] Jianfeng Huang, Mounir Mensi, Emad Oveisi, Valeria Mantella, and Raffaella Buonsanti. Structural sensitivities in bimetallic catalysts for electrochemical co_2 reduction revealed by ag–cu nanodimers. *Journal of the American Chemical Society*, 141(6):2490–2499, 2019.

[73] Xiaoying Han, Zhihui Yu, Jingkui Qu, Tao Qi, Wei Guo, and Guoqing Zhang. Measurement and correlation of solubility data for co_2 in $nahco_3$ aqueous solution. *Journal of Chemical & Engineering Data*, 56(4):1213–1219, 2011.

[74] Wenbo Ju, Juqin Zeng, Katarzyna Bejtka, Huan Ma, Daniel Rentsch, Micaela Castellino, Adriano Sacco, Candido F. Pirri, and Corsin Battaglia. Sn-decorated cu for selective electrochemical co_2 to co conversion: Precision architecture beyond composition design. *ACS Applied Energy Materials*, 2(1):867–872, 2018.

[75] Daniel S. Ripatti, Thomas R. Veltman, and Matthew W. Kanan. Carbon monoxide gas diffusion electrolysis that produces concentrated c_2 products with high single-pass conversion. *Joule*, 3(1):240–256, 2019.

[76] S. Park, J.-W. Lee, and B.N. Popov. A review of gas diffusion layer in pem fuel cells: Materials and designs. *International Journal of Hydrogen Energy*, 37: 5850–5865, 2012.

[77] Byoungsu Kim, F. Hillman, M. Ariyoshi, S. Fujikawa, and P. J. A. Kenis. Effects of composition of the micro porous layer and the substrate on performance in the electrochemical reduction of co_2 to co. *Journal of Power Sources*, 312:192–198, 2016.

[78] R. L. Cook, R. C. MacDuff, and A. F. Sammells. High rate gas phase co_2 reduction to ethylene and methane using gas diffusion electrodes. *Journal of The Electrochemical Society*, 137(2):607–608, 1990.

[79] David M. Weekes, Danielle A. Salvatore, Angelica Reyes, Aoxue Huang, and Curtis P. Berlinguette. Electrolytic co_2 reduction in a flow cell. *Accounts of Chemical Research*, 51(4):910–918, 2018.

[80] Charles Delacourt, Paul L. Ridgway, and John S. Newman. Mathematical modeling of co_2 reduction to co in aqueous electrolytes: I. kinetic study on planar silver and gold electrodes. *Journal of the Electrochemical Society*, 157(12):B1902–B1910, 2010.

[81] Blanka Endrődi, Gergely Bencsik, Ferenc Darvas, Robert Jones, Krishnan Rajeshwar, and Csaba Janáky. Continuous-flow electroreduction of carbon dioxide. *Progress in Energy and Combustion Science*, 62:133–154, 2017.

[82] Francesco Seller, Davide Arcoraci, Pietro Zaccagnini, Alessandro Cultrera, Micaela Castellino, Marco Allione, Mara Serrapede, and Andrea Lamberti. Electrochemical deposition of copper (111) on carbon nanotubes yarns. *SSRN Electronic Journal*, page 16, 2025.

[83] Felicia Di Costola, Nicolò B.D. Monti, Ilargi Napal, Elena Magnano, Candido F. Pirri, Giancarlo Cicero, Marco Fontana, Francesca Risplendi, Silvia Nappini, and Juqin Zeng. Unveiling ag-modulated cu active sites for enhanced multicarbon product formation in co_2 electroreduction. *The Journal of Physical Chemistry Letters*, 16:9088—-9096, 2025.

[84] Dehua Ren, Yuhan Deng, Andi D. Handoko, Chia-Sheng Chen, Subhash Malkhandi, and Boon S. Yeo. Selective electrochemical reduction of carbon dioxide to ethylene and ethanol on copper(i) oxide catalysts. *ACS Catalysis*, 5(5): 2814–2821, 2015.